

Evaluation of transient lift loads
during a decommissioning
operation with a crane vessel

P.M. Jacobs



Evaluation of transient lift loads during a decommissioning operation with a crane vessel

by

P.M. Jacobs

in partial fulfilment of the requirements for the degree of

Master of Science

in Offshore and Dredging Engineering
at the Delft University of Technology

The logo for TU Delft, featuring a stylized flame icon above the text "TU Delft".The logo for Boskalis, featuring a crown icon above a yellow and blue square, followed by the text "Boskalis".

Student number:	4006879
Project Duration:	September, 2016 – July, 2017
Thesis Committee:	Prof. Dr. A.V. Metrikine TU Delft, chairman
	Ir. C. Keijdener TU Delft
	Dr. ir. K.N. van Dalen TU Delft
	Ir. P. Antonakas Boskalis
	Ir. P. Hendrickx Boskalis

This thesis is confidential and cannot be made public until July 12, 2022.

An electronic version of this thesis is available at <http://repository.tudelft.nl/>.

With the conversion of a heavy transport vessel into a crane vessel, Boskalis aims to strengthen its position in the offshore wind and decommissioning markets. The BOKALIFT 1, as the crane vessel will be named, is equipped with a 3,000 tonne crane and a class-2 Dynamic Positioning system. In order to utilise its exceptional large and strong deck area to its full extend, the crane is installed amidships at the starboard side of the vessel (see Figure 1). Offshore lifts are consequently performed in transverse direction of the vessel, resulting in a large heeling moment during the lift operation. As the conversion is currently ongoing no operational experience has been gained yet. This thesis is therefore an assessment on the behaviour of this new asset and the crane loads during a lifting operation close to the maximum crane capacity. This is the case for a single-lift decommissioning operation, lifting a topside from a jacket support structure.



Figure 1 - Impression of the BOKALIFT 1 during a decommissioning operation

Two transient phenomena can occur throughout the decommissioning operation: snap loads and impact loads (see Figure 2). Both phenomena cause large peaks in the crane loads. Snap loads occur in the rigging lines during the pre-tensioning. During this phase the rigging lines become taut and the motions of the crane hook are constrained. Impact loads can occur during the final lift phase of the topside. This phase is estimated to last several minutes and is driven by the capacity of the dedicated anti-heeling system. Its purpose is to compensate the large heeling moments. Since this operation will last multiple wave periods, the wave induced motion at the crane tip causes tension variations in the hoisting system. When this tension exceeds the required lift tension the topside is temporary lifted, with impact loads as a result.

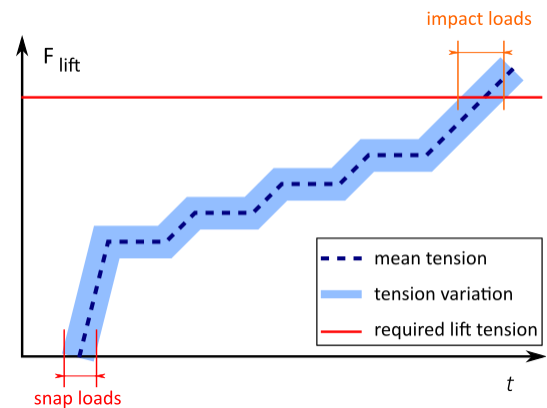


Figure 2 - Qualitative representation of the tension in the hoisting system throughout the full operation

An OrcaFlex model is built to perform time domain simulations of the pre-tensioning and lift phases of the decommissioning operation for several irregular sea states. For both phases, a crane load comparison is conducted for two different lifting schemes. In the first scheme the hoisting speed is dictated by the anti-heeling system in order to maintain even-keel conditions. This is favourable for the operation limits. For the second scheme this is disregarded and the maximum hoist speed is applied. The latter is expected to reduce the duration where impact loads are present.

In the pre-tensioning phase, the higher hoisting speed results in a larger amplitude of the load variation since the snap loads are dictated by the relative velocity of the crane hook. During the lift phase, the higher hoisting speed reduces the time during which impact loads occur and thereby also reduces the crane loads. However, the topside motions are significantly increased. The crane tip- and topside motions have shown to be the limiting criteria for the lift operation. Limiting the topside motions by bumpers, guides or extra tugger lines can increase the workability for sea states where the peak period is close to the vessels natural heave and pitch period. Conclusively this thesis shows that the BOKALIFT 1 is a very well-suited vessel for offshore decommissioning operations.

List of Abbreviations

Abbrev.	Description:
AH	Anti-Heeling
CL	Centre Line
CoG	Centre of Gravity
DAF	Dynamic Amplitude Factor
DHL	Dynamic hook load
DP	Dynamic Positioning
PS	Portside
RAO	Response Amplitude Operator
SB	Starboard
SHL	Static Hook Load
TCG	Transverse Center of Gravity
TS	Topside
VCG	Vertical Center of Gravity

Table of content

	Abstract.....	iii
Chapter 1.	Introduction	1
	1.1. BOKALIFT 1	1
	1.2. 3,000 t Offshore Mast Crane	2
	1.3. Thesis scope	3
	1.4. Decommissioning	3
	1.5. Problem identification	6
	1.6. Objectives	10
	1.7. Methodology	11
Chapter 2.	Modelling and system properties	13
	2.1. General arrangement	13
	2.2. Vessel and Response Amplitude Operators	15
	2.3. Hoisting system	16
	2.4. Anti-heeling system	18
	2.5. Horizontal vessel constraints	20
	2.6. Topside and substructure interface	20
	2.7. Conclusion	22
Chapter 3.	Modal analysis.....	23
	3.1. Mode shapes	23
	3.2. Natural periods	27
	3.3. Conclusion	28
Chapter 4.	Tension variation and set-up of transient time-domain simulations	29
	4.1. Environmental conditions	29
	4.2. Even keel conditions	30
	4.3. Tension variation and workability	31
	4.4. Pre-tensioning the hoisting system	32
	4.5. Lift of the topside	33
Chapter 5.	Results transient time-domain simulations.....	35
	5.1. Pre-tensioning simulations	35
	5.2. Lift simulations	38
Chapter 6.	Conclusions and recommendations.....	43
	References	45
Appendix A.	OrcaFlex.....	49
Appendix B.	Diffraction analysis.....	51
Appendix C.	Results	57

Chapter 1. Introduction

Boskalis is a large and widely known dredging company with over a century of experience, originating from The Netherlands. Historically, land reclamation and coastline protection have always been core activities. By several acquisitions during the last two decades, it broadened their scope of work. Nowadays Boskalis has a large variety of assets which are deployed as a marine service provider active in the markets of offshore energy, salvage and towage, next to the dredging market.

The offshore energy sector is subject to change due to transition towards renewable energy sources and the drop of the oil price in the recent years. New activities are the large-scale offshore wind farm installation and the removal of retired production facilities, decommissioning. Boskalis aims to improve its market position in the offshore energy sector with a new, complementary asset, that will be the main character in this thesis.

1.1. BOKALIFT 1

Boskalis is currently working on the conversion of an F-class Semi-Submersible Heavy Transport Vessel into a Heavy Lift Vessel (see Figure 1-1 and Figure 1-2) which will be named “BOKALIFT 1”. Huisman Equipment B.V. received the order to build and install an offshore mast crane that is capable of lifting cargo up to 3,000 metric tonnes and which is expected to be delivered by the end of 2017 (Heavy Lift PFI, 2016). Next to the installation of the offshore mast crane, the vessel conversion includes the fitting of a class-2 Dynamic Positioning (DP) system. It is intended to become an important asset for Boskalis’ future offshore wind farm installation and offshore decommissioning projects.



Figure 1-1 F-class Semi-Submersible Heavy Transport Vessel Finesse



Figure 1-2 Artist impression Heavy Lift Vessel BOKALIFT 1

Due to its origin as Heavy Transport Vessel the BOKALIFT 1 has a very strong and large deck space of which 165 by 43 meters is available for cargo after the installation of the mast crane (Boskalis, 2017). This is outstanding compared to similar heavy lift vessels owned by Jumbo (up to 3,250 m², (Jumbo Maritime, 2016)) and Seaway Heavy Lifting (up to 3,700 m², (Seaway Heavy Lifting Engineering B.V., 2016)). To make efficient use of this important characteristic, the crane will be installed at an atypical location: halfway the deck length at the (starboard) side of the vessel. With a reach of the main hoist of 70 meters the crane is able to cover the full deck space.

1.2. 3,000 t Offshore Mast Crane

Huisman Equipment B.V. is a well-known name within the (Dutch-) offshore industry and has a good record as crane manufacturer. The most famous crane type is the tub mounted crane, as world's largest crane vessels of the last decades are equipped with those. Heerema Marine Contractors' Thialf (in use since 1985) and the Saipem 7000 (in use since 1987) are also equipped with tub mounted cranes. The next world's largest crane vessel is currently under construction by Heerema Marine Contractors and will have two Huisman tub mounted cranes installed with a capacity of 10,000 metric tonnes each (see Figure 1-3).



Figure 1-3 World's largest crane vessel – Sleipnir (Heerema Marine Contractors)

A downside of this crane type is that it has a very large footprint on the vessel deck compared to other crane types. For the markets that Boskalis is aiming at with the BOKALIFT 1, optimal use of the available deck space and operational handling speed is more important than a high lifting capacity, especially for the offshore wind farm installation projects. Therefore an Offshore Mast Crane is chosen, shown in Figure 1-4. Like the tub mounted crane, this crane type is able to rotate around its slewing platform (see Figure 1-5 for nomenclature of the crane elements).



Figure 1-4 Huisman Offshore Mast Crane (Huisman Equipment B.V., 2015)

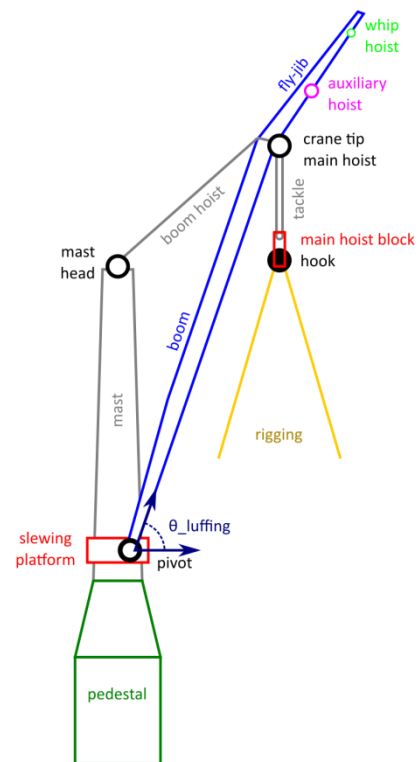


Figure 1-5 Crane nomenclature

1.3. Thesis scope

As the BOKALIFT 1 is still under construction by the time of this study, no operational experience is available for future projects. This thesis can therefore be seen as an initial engineering study into the behaviour of this new asset when performing at its full extend. Since the crane has an offset towards starboard with respect to the centre line of the vessel, the vessel will be subject to large heeling moments during offshore lifting operations. The largest heeling moment that the vessel will encounter is obtained when the asset is performing a lift operation at the maximum crane capacity at a maximum outreach. These conditions are met during a decommissioning operation, which is the scope of this thesis. At several stages during this operation the vessel behaviour and the loads on the crane are investigated. The configuration that will be focussed on consists of a topside supported by a jacket substructure. During the operation the topside will be lifted off its support in a single piece. Detailed information regarding this setting are provided by Boskalis.

1.4. Decommissioning

Decommissioning can be defined as the process of removal of a disused offshore production facility, starting at the moment of shutting down the production and ending when the facilities are physically removed. International legislation regarding the offshore energy market is established in international and regional conventions, guidelines and national laws. Decommissioning was mentioned for the first time during the first United Nations Conference on the Law Of the Sea (UNCLOS) held in Geneva, 1958. One of the products of this conference is the Convention on the Continental Shelf, which states that: “*any installations which are abandoned or disused must be entirely removed*” (UNCLOS, 1958). Since this convention slight amendments are made to the obligation of the *entire* removal of abandoned installations regarding the feasibility and the effect on the marine environment of the removal (Martin, 2003).

Following the guidelines from IMO Resolution A. 672(16) (International Maritime Organisation, 1989), the obligation for removal applies to structures that are in water depths smaller than 75 meter, with a mass less than 4,000 tonnes (excluding topsides). Other structures have to be partially removed to 55 meter below the water surface. To make decommissioning easier in the future all structures installed from 1 January 1998 onwards should be designed such that entire removal is feasible. One of the regional conventions of the international legislation that not only adopted, but even strengthened the IMO Resolution is the OSPAR Decision 98/3 (OSPAR Commission, 1998), which applies to the North-East Atlantic. This convention prohibits the disposal (even the partial) unless derogation is granted, leaving no choice for at least considering the entire removal. Next to that, all structures with a mass smaller than 10,000 tonnes are obliged to be fully removed.

In contrast to Europe, at other parts of the world the amendments to the obligation of entire removal are interpreted more literally. In the United States, there have been over 400 abandoned structures left in place and converted to artificial reefs under the rigs-to-reefs program (Gourvenec & Techera, 2016). This decommissioning alternative for the total removal of the offshore structures is described by (Macreadie, Fowler, & Booth, 2011) are shown in Figure 1-6. The rigs-to-reefs alternatives consist of (a) leaving the structure in place, (b) toppling the structure on site, (c) fulfilling the IMO free-clearance criteria by cutting off the top of the structure and lowering it to the seabed, and (d) towing the structure to a more appropriate location before sinking it.

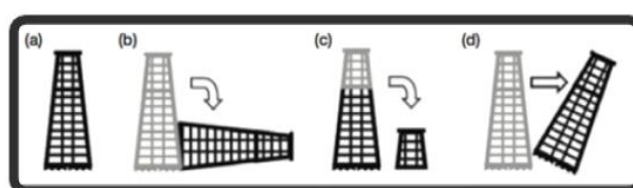


Figure 1-6 Alternative decommissioning options (Macreadie et al., 2011)

1.4.1. Methods

Considering decommissioning as the part of the physical removal of the production facilities only, there are various methods to perform such an operation. Looking at decommissioning limited to facilities with a steel bottom founded substructure, the topsides and the substructure are separated during the operation. The decommissioning methods listed below apply to topsides (Decom North Sea, 2014, 2015):

- **Single-lift:** cutting the connection between the topside and its substructure and lifting the topside in one piece
- **Reverse installation:** cutting the connection between the topside and its substructure and perform a reverse float-over installation of the topside in one piece using buoyancy modules or barges
- **Heavy lift:** removing the topside per module in the reverse sequence of installation
- **Piece small:** cutting the topside modules in small pieces that can be handled by the platform cranes (i.e. up to 20 tonnes) and fit into containers for transport to shore

Regarding the decommissioning of the steel jackets, the decommissioning methods are very similar to the methods listed above, except for the piece small method which is not applicable. However, the principle of cutting the jacket into pieces is used, but since the pieces are to be lifted by a crane vessel the pieces have weights that are in the range of the heavy lifting method. The reverse installation method for jackets is performed by attaching buoyancy modules.

1.4.2. Market

As stated in the introduction of this section, the restrictions to remove retired platforms are most strict in the North Sea. Over 550 platforms are to be decommissioned in the next 30 years, many of which within 10 years (see Figure 1-7). According to (Gourvenec & Techera, 2016), the Southeast Asian decommissioning market will soon open up, as half of the region's 1700 offshore installations are in production for over 20 years and are close to the end of the field life.

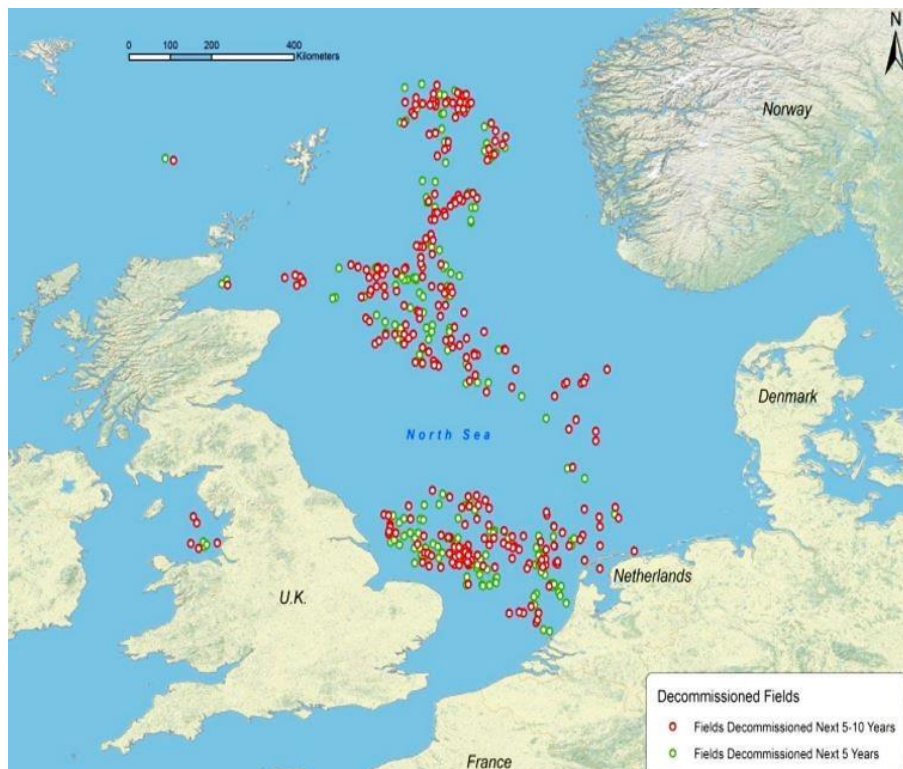


Figure 1-7 Fields to be decommissioned in the near future (Palantir, 2014)

1.4.3. Decommissioning at Boskalis

Current decommissioning operations of topsides and substructures at Boskalis are performed by Floating Sheerleg Vessels (Figure 1-8). These barge-shaped vessels have a fixed A-frame crane at the stern, with lifting capacities ranging from 400 to 5,000 tonnes (Boskalis, 2016a) and perform decommissioning operations using the single-lift and heavy lift methods. Transportation of a decommissioned topside or substructure is done by loading it onto an additional barge or ship or by carrying the lifted object in the hook during transit.



Figure 1-8 Boskalis' floating sheerleg vessels Taklift 4 and Taklift 7

Vessels without DP capabilities, like the floating sheerleg vessels, require a mooring system to be kept in place. The design of such a system should be adapted for each project, based on the offshore site characteristics as the water depth and the environmental conditions. Next to that, the large footprint of a mooring system has to be taken into account during the engineering, which might be complicated due to the infrastructure that is present on the seabed. Installing the mooring lines requires (anchor handling-) tugs and therefore obtaining the desired vessel position and orientation is more time consuming when using a mooring system compared to a dynamic positioning system.

Like the presence of anchor handling tugs is no longer needed as a consequence of using DP, barges are no longer required for the operation as the BOKALIFT 1 accommodates the deck space required for the transportation of the offshore structures that are to be installed or decommissioned. The use of the deck space, in return, is facilitated by the adjustable orientation of the offshore mast crane. Conclusively, from an operational and logistical point of view, less valuable time is needed for lift operations using the BOKALIFT 1 and less assets are needed which makes the organisation of lift operations less complicated, and thereby safer.

1.4.4. A decommissioning operation with the BOKALIFT 1

As the conversion of the BOKALIFT 1 is ongoing, no experience is available on decommissioning projects executed by the vessel. Regarding a single-lift decommissioning operation, the proposed working method consists of the following steps:

0. Preparations (engineering)

In order to make the removal of an offshore production facility a safe operation, several preparations have to be made before the vessel can go out to do the job. Independent of the decommissioning method chosen, the

platform is visited beforehand to detect weak spots of the structure and investigate the overall (structural) condition it is in. Depending on the proposed method of decommissioning more or fewer engineering calculations have to be performed regarding the structural integrity/strength of the platform during the decommissioning operation.

1. Preparations (on-site)

Upon approval for the execution of the operation the vessel is located at the right position. The positioning is subject to regulations regarding minimal clearances between the vessel, the mooring system (if present) and the offshore structure (Det Norske Veritas, 2014a). After obtaining the right position, station keeping is performed by using a mooring system or by Dynamic Positioning. With the vessel in-place, the crane is turned until its tip is located right above the topside, after which the rigging can be attached to the topside and the crane hook.

2. Pre-tensioning of hoisting system

The tension in the hoisting system, consisting of the main hoist tackles and the rigging lines, is increased quickly by reducing the tackle length of the main hoist and by transferring ballast water from starboard to portside between designated tanks. The latter is performed by a dedicated anti-heeling system. The heeling moment that the transferred mass of the ballast water provides an increases the tension in the hoisting system. This is done in order to have the topside under tension, thus connected to the vessel, before the cutting of the legs connecting the topside and the jacket substructure is started.

3. Cutting of the legs

With the topside under tension of the crane, the legs that connect the topside and substructure are cut. If the facility allows, an internal cutting tool is lowered into the leg in order to perform the cutting. Hereby the cut is made mechanically, remote controlled. This system is able to add a certain geometry to the shape of the cut. When this is not possible the cut can be made from the outside. This cut is man-made using a fire torch. Between the cutting of two legs the tension in the hoisting system can be increased stepwise.

4. Redistribution of topside load

When the last leg has been cut, the topside weight is still partly supported by the substructure. The final redistribution of the topside load from the substructure to the hoisting system is driven by the anti-heeling system.

5. Lift and Transport

At the end of the redistribution of the topside load to the hoisting system, the topside is lifted to a preferred height using the winches of the main hoist lines. After that, the crane is able to turn and lower the topside onto the intended location on the deck.

At several moments in time throughout this operation, motions of the vessel and topside and crane loads have to be evaluated in order to make sure this operation is a safe one, both for personnel and the assets used. The threads expected to occur encountered are discussed in the next section.

1.5. Problem identification

The description of the decommissioning operation given in the previous section can be seen as a series of snapshots in time, describing the lifting process in a static manner. Investigating a continuous time interval leads to several prompt changes in the description of the dynamic vessel-topside system, and the interaction with the environment has to be accounted for. Due to this interaction, a part of the environmental energy is transferred

to the rigid bodies through forces, resulting in body motions. The dynamical behaviour of the vessel-topside system and its complications with respect to the decommissioning operation are discussed in this section.

1.5.1. Configurations of the dynamic vessel-topside system

Considering the vessel, the hook at the main hoist block and the topside as rigid bodies which have 6 degrees of freedom, three dynamical descriptions of the vessel-topside system behaviour during a decommissioning operation can be distinguished. The configurations before attaching the rigging lines to the hook, during the redistribution of the topside load and after the lift of the topside are described in succession.

Configuration 1: Uncoupled system

Before attaching the hoisting system to the topside, there is no connection between the vessel and the topside and thus their motions are uncoupled. The vessel behaves as a free floating body and is subject to environmental forces, having its motions only constrained by the station keeping system. The main hoist block and the hook are free to move like a pendulum, which is hinged at the crane tip. At this point in time the topside is rigidly connected to the fixed, bottom founded jacket substructure. The environmental loads acting on the topside and substructure are transferred through its foundation piles into the soil. The stiffness of the substructure is such that the motions of the topside are negligible small.

Configuration 2: Constraint system

Attaching the rigging lines to the hook connects the rigid bodies of the topside and the vessel. Since the topside is still rigidly connected to the substructure, this connection only affects the vessel motions. The connection can be seen as an additional constrain next to the station keeping. By pre-tensioning the hoisting system the rigging lines are taut, which changes the (slack hanging rigging lines) connection to a semi-rigid constrain to the displacement of the main hoist block and the hook. Thereby the vessel motions are constrained at the crane tip, which can only move in the horizontal plane. Crane tip motions in the vertical direction require elongation of the hoisting wires. Hereby, the centre of rotation of the vessel is shifted to the hook. In this constraint configuration the anti-heeling system slowly increases the tension in the hoisting system and the legs connecting the topside and the substructure are cut one by one.

Configuration 3: Coupled system

By cutting the last leg, the topside is no longer rigidly connected to the substructure. The lift of the topside can now be performed and affects the dynamic behaviour of the vessel, as it is no longer semi-rigidly fixed at the crane tip when the topside is no longer supported by the substructure. The hoisting system and the topside mass acts as a pendulum, hinged at the crane tip. Due to the wave-induced motions of the vessel the hinge moves. As a consequence the topside will translate and rotate in the horizontal plane. Next to the pendulum behaviour, the topside is allowed to heave (relative to the crane tip, in the direction of the pendulum) since the hoisting system should be considered as a tether (a spring that can only take tension due to elongation). Through this tether the motions of the topside – not only the heave motion – exert forces in varying directions on the crane tip, thereby affecting the vessel motions. Therefore the vessel and topside motions are dynamically coupled after the lift of the topside.

1.5.2. Variation of tension in the hoisting system

Accounting for the excitation of the vessel due to environmental loads introduces motions of the vessel in all degrees of freedom. As a consequence of the location of the crane amidships at starboard and the loading in the transverse direction of the vessel, heave and roll are the most important vessel motions for the lifting process. The motions in these degrees of freedom result in a variation of the vertical position of the crane tip. The energy of these motions is translated into a variation in tension in the hoisting system when the dynamic vessel-topside

system is semi-rigidly constraint. Physically this variation in tension means a variation of the elongation of the hoisting wires in time.

A qualitative representation of the mean tension in the hoisting wires during the process is given by the dotted line in Figure 1-9. The figure consecutively shows the phases of the quick pre-tensioning of the hoisting wires by the reduction of the tackle length, the alternating cutting of a topside leg and redistributing the topside load to the vessel and the final lift of the topside, the latter two driven by the anti-heeling system. The tension variation is represented by the light blue area around the dotted line of the mean lifting tension. This introduces two phenomena: snap loads in the rigging lines at the start of the pre-tensioning and impact loads of the topside to the substructure during the final lift of the topside.

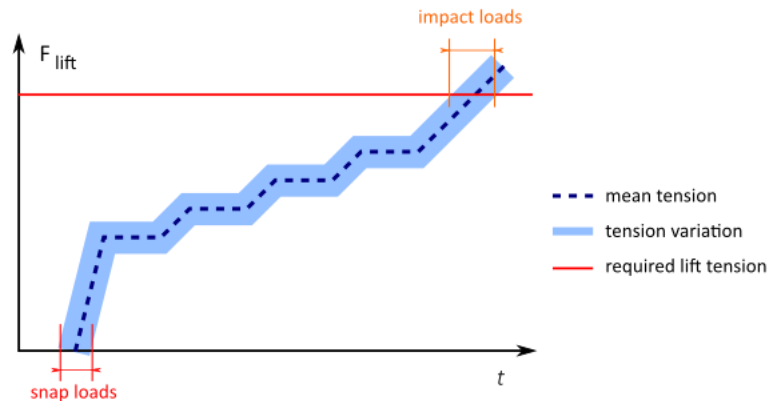


Figure 1-9 Qualitative representation of the tension in the hoisting wires over decommissioning process

1.5.3. Snap loads

Snap loading of a wire rope is often referred to in combination with dropped objects connected to one of its ends. The phenomenon describes the wire rope from a slack or loose condition to a (temporarily) taut condition due to the falling object. The amplitude of the snap load is the maximum tension in the rope, which occurs when the maximum elongation of the rope has reduced the velocity of the falling object to zero. Next to the static force and the corresponding static elongation in the wire rope due to the weight of an object there is a dynamic force due to a tensile stress wave due to the impact of the dropped object. This force depends on the velocity at which the object starts to elongate the wire rope, the initial velocity (Irvine, 1981):

$$F = m_T \cdot c \cdot v_0 \cdot e^{(-m_T \cdot c \cdot t)/M} \quad \text{where } c = \sqrt{E/\rho} \quad (1.1)$$

where m_T is the mass of the wire rope per meter in [kg/m], c is the wave velocity [m/s], v_0 is the initial velocity [m/s], M is the mass of the dropped object in [kg], t is the time in [s], E is the elasticity modulus or Young's modulus in [N/m²] and ρ is the density of the rope in [kg/m³]. It must be noted that the magnitude of the snap load does not depend on the mass of the object but solely on its initial velocity. Only the decay of the snap load is influenced by this mass.

Snap loads are unfavourable since these can cause serious wear to the wire rope which shortens the fatigue lifetime. Also local failures can occur in the outer wires of the rope and so-called bird caging can occur due to the quick elongation (Balmoral Marine, 2004). During the decommissioning operation, snap loads can occur at the interface between the uncoupled and the constraint system as described in the previous section.

Since the hoisting wires are tensioned due to the self-weight of the main hoist block and the hook, the snap loads will occur in the rigging lines when going from a slack to a taut condition. With slack rigging lines, the main

hoist block and crane hook are free to move in vertical direction corresponding to the motion of the crane tip. As the hook is lifted during the pre-tensioning by decreasing the tackle length, the rigging will start to prevent the hook from moving upwards at a certain moment. The “dropped” object in this case therefore is the hoist block and the hook of the hoisting system. In the hoisting wires this also exerts a tensile stress wave from the hoist block to the crane tip. As the wear of the rigging lines is not as relevant as it is for the hoisting wires – the rigging is specifically designed for the operation – the threads left are due to local failure. Besides the tensile strength of the rigging lines also the padeyes on the topside should be strong enough to cope with the snap loads.

Snap loads will repeatedly occur until the vertical motions of the crane tip are translated into tension variation as indicated in Figure 1-9, thus until the mean tension in the wire ropes is larger than the amplitude of the tension variation. A quick increase of tension in the hoisting system is to be achieved by reeling in the wire rope by the winches of the crane.

1.5.4. Impact loads

Impact loads are defined here as the forces that occur as a consequence of the topside hitting the substructure. These are expected to occur at the transition between the constraint and the coupled configurations of the dynamic vessel-topside system as described earlier in this chapter, due to the speed of the redistribution of the topside load from the substructure to the vessel, which is driven by the anti-heeling system. The pumps used in this system have a limited capacity, thereby limiting the speed of the load redistribution. The lift phase is expected to last several minutes. This causes impact loads at the cut interface on the topside and the substructure. Consequently a drop of tension in the hoisting system occurs, exerting loads and on the crane tip. This interface, in time, is here defined as the transient lift phase.

The impact loads are a consequence of the tension variation. At a certain moment in time, the sum of the mean lift load and the amplitude of the tension variation reach the required lift load to lift-off the topside from the substructure. Physically this occurs when the crane tip is moving upwards due to the heave and roll motions of the vessel. When the crane tip moves downwards, the required lift load is no longer met in the hoisting system, causing the topside to be lowered onto the substructure legs with a certain velocity. The topside continues to hit the substructure until the mean lift load is larger than the sum of the required lift load and the tension variation.

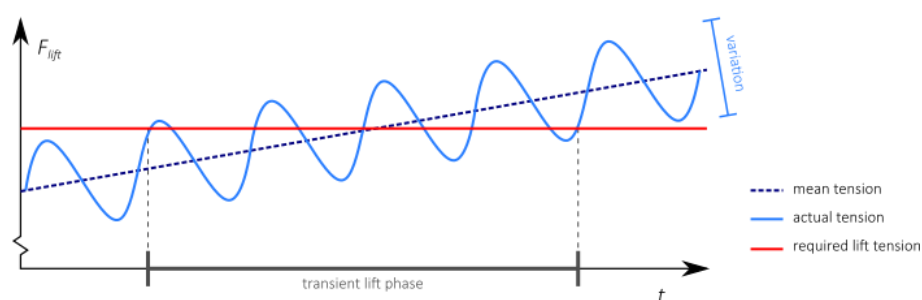


Figure 1-10 Qualitative representation of the impact load phenomenon

In Figure 1-10 a representation of the tension in the hoisting system is given. Since the tension is drawn as a harmonic, one can understand that this is a qualitative representation. The moments of impact are the downward crossings of the lift load through the line indicating the required lift load. The upward crossings are the moments of lift-off. Physically the overshoot in tension does not occur, here the topside is temporarily lifted. In reality the motions of the crane tip, which induce this variation, is a combination of the vessel motions which have different periods, amplitudes and phases. Next to that, the waves exciting the vessel are not harmonic as well.

1.6. Objectives

The focus in this thesis is on the behaviour of the coupled vessel-topside system during the transient snap- and impact loads that are expected to occur during a single-lift decommissioning operation. These loads are to be evaluated by a time domain motion analysis model that accounts for the coupled dynamics of the sea-excited vessel and the topside. The main objective of this thesis reads:

“Evaluate the behaviour of the BOKALIFT 1 during the transient phases of a decommissioning operation”

The sub-objectives described below are the aspects that give insight in the behaviour of Boskalis’ new asset, the BOKALIFT 1, during a decommissioning operation.

To be more specific, the location where those loads are evaluated is at the crane tip, as the crane loads are determining the workability limits of the vessel. Following the decommissioning operation from pre-tensioning to the lift of the topside several limits have to be defined. As discussed in the previous section, both transient phenomena depend on the crane tip motions and the tension variation in the hoisting system. Before the cutting of the first leg can start, the snap loads have to be overcome. Accordingly, the impact loads should not occur right after the last cut has been made. Therefore a range of tension in the hoisting system can be defined during which the cutting can safely be executed, accounting for the transient phenomena and the amplitude of the tension variation.

When the tension variation is known the pre-tensioning- and lift simulations can be prepared, which result in criteria for the workability of the vessel. Next to the evaluation of the crane loads on its limits, which defines the workability, different lifting speeds are investigated. For the pre-tensioning simulations this involves a simulation at which the lifting speed is maximal, after which the anti-heeling system compensates the static roll angle and a simulation at which lifting speed is dictated by the ballasting speed of the anti-heeling system in order to keep the vessel at even keel conditions.

Regarding the lift simulations, the redistribution of loads is proposed to be driven by anti-heeling system. Here, moment at which the maximum hoisting speed is applied will be varied. Another sensitivity analysis on impact loads is regarding the type of leg cut used, as the geometry of the machine-made cuts can be seen as small guides for the lift operation. For all lift simulations the motion of the free hanging topside is investigated regarding motion- and clearance criteria. If these are not met the topside should be guided by a temporary structure during the transient lift phase or bumpers should be installed.

Conclusively, a summary of the sub-objectives is given:

- Determine the range of tension in the hoisting system where the transient phenomena of snap loading and impact loads can occur. Hereby also the range of tension during which the jacket legs can safely be cut is defined.
- Investigate whether the hoisting speed influences the crane loads caused by the transient phenomena
- Check whether or not additional precautions are necessary to limit the motions of the topside during the lift phase for certain sea states
- Investigate whether the type of leg cut influences the topside motions and the crane loads during the lift phase

1.7. Methodology

The evaluation of the behaviour of the BOKALIFT 1 during the transient phases of a decommissioning operation is performed by taking the following steps:

1. Modal analysis

In order to get a closer look into the vessel behaviour, a modal analysis is performed to investigate the natural periods of the configurations of the vessel-topside system at different stages during the decommissioning operation. The three configurations described in the problem identification are assessed. Based on this analysis, critical wave loading periods and the coupling between degrees of freedom are identified.

2. Time domain simulations to define the tension variation

As the transient snap loading and impact phenomena occur depending on the level of tension in the hoisting system, the tension variation is assessed for several tension levels. As the cutting of the legs will be a time-expensive operation, a 3 hour simulation per sea state is required by the regulations to define the maximum amplitude of this variation (Det Norske Veritas, 2007). With the amplitude of the tension variation identified, the operating window for the cutting is known. Stated otherwise, this defines the end of the pre-tensioning phase and the start of the lift phase.

3. Time domain simulations pre-tensioning and lift of the topside

As these are short operations, i.e. in the order of minutes, multiple simulations are required to estimate the maximum crane loads. Based on the maximum crane loading criteria and motion criteria, which are defined in the next chapter, the workability is examined. For both the pre-tensioning and lifting simulations the effect of a different lifting speed on these criteria is evaluated. Next to that, two different cut types are examined in the lift simulations.

Chapter 2. Modelling and system properties

In order to evaluate the transient response of the vessel-topside system, the system is modelled in OrcaFlex, a multi-body dynamic analysis program for offshore marine systems. A brief description of the different modelling elements available can be found in Appendix A. The modelling of the different aspects of the dynamically coupled vessel-topside system is discussed in this chapter. To start with, a description of the arrangement for the decommissioning operation is given. This is followed by a discussion on the vessel model, the anti-heeling system, the mast crane and the station keeping system. The model for the decommissioning arrangement is completed by the topside and the cut interface of the jacket legs. A preview of the model can be seen in the figure below.



Figure 2-1 OrcaFlex model

2.1. General arrangement

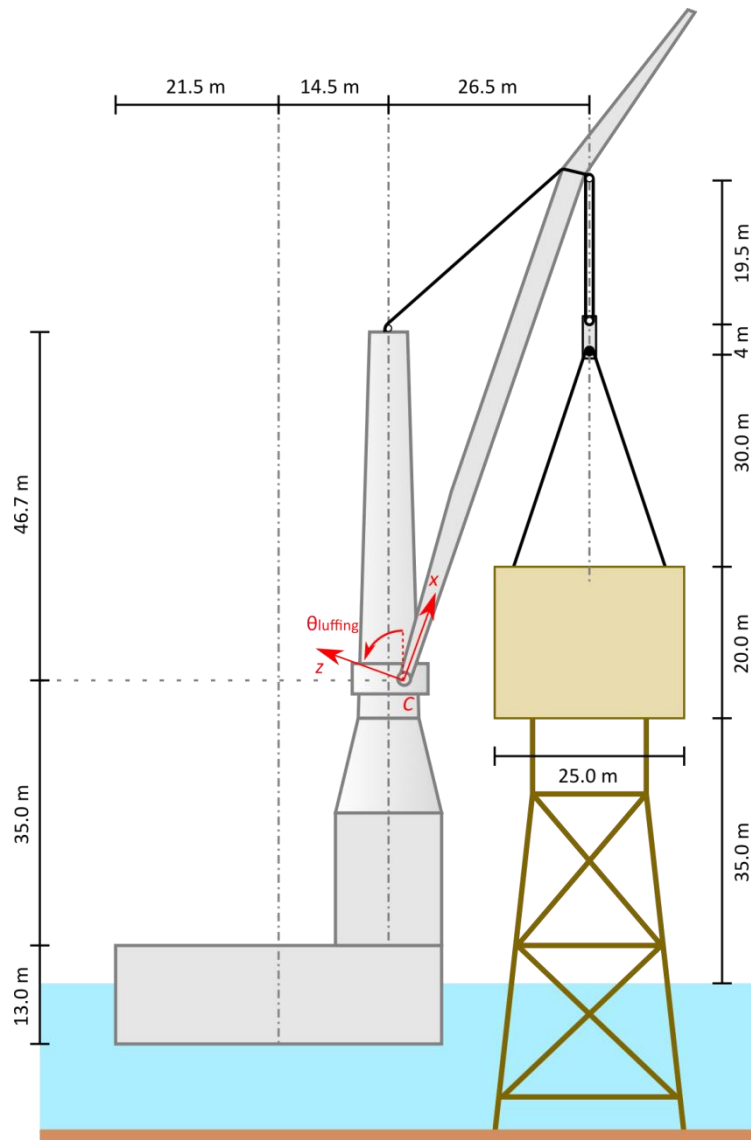
Recalling the scope of this thesis, the decommissioning operation that is to be considered should result in a maximum heeling moment in order to evaluate the vessel behaviour during the transient lift phase. This results in a combination of crane outreach and weight of the object which is to be lifted, as long as this load fits within the safe working load crane diagram. The dimensions are presented in the tables below and in Figure 2-2. The location of the crane on the vessel can be seen in the general arrangement of the BOKALIFT 1 in Figure 2-3.

Table 2-1 General arrangement decommissioning operation

Crane outreach	26.5	m
Height crane tip	105.5	m (wrt MWL)
Main Hoist tackle length	19.5	m
CoG Topside wrt vessel CL	41.0	m
Topside mass	2,500	t
Rigging + hoist block mass	300	t

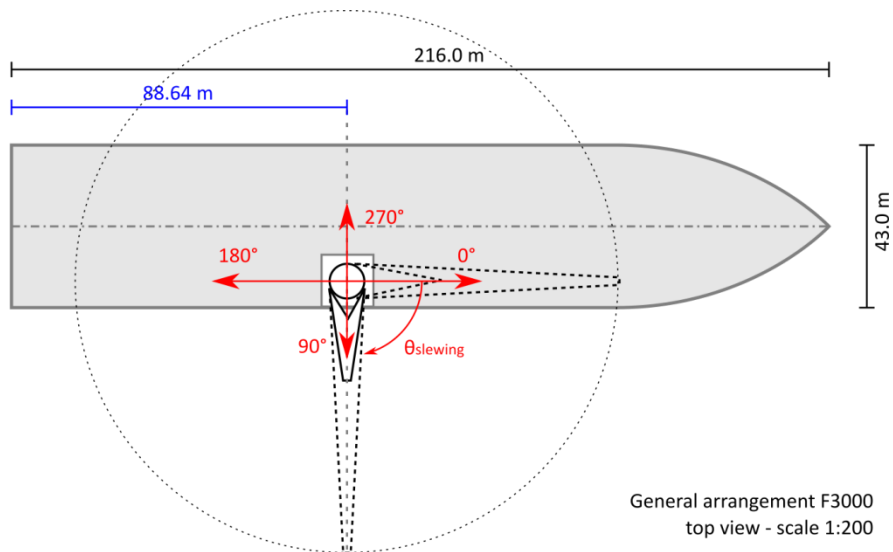
Table 2-2 Particulars BOKALIFT 1

Length	216.0	m
Breadth	43.0	m
Depth	13.0	m
Draft during operation	8.0	m
Deck space [L x B]	165 x 43	m
Deadweight	50,000	t



General arrangement F3000
side view - scale 1:100

Figure 2-2 General arrangement decommissioning operation



General arrangement F3000
top view - scale 1:200

Figure 2-3 General arrangement BOKALIFT 1 and mast crane

2.2. Vessel and Response Amplitude Operators

Response Amplitude Operators (RAO) are used in OrcaFlex to calculate the response of a floating rigid body due to wave excitation. An RAO is a transfer function that relates an incoming regular harmonic wave, which has a certain wave amplitude, frequency and direction (with respect to the vessel orientation), to the harmonic vessel response. Per wave frequency the RAO is calculated for each degree of freedom of the vessel separately, and consists of an amplitude and a phase. There are two types of RAO. Displacement RAO directly relate the amplitude of the incoming harmonic wave to the amplitude of the harmonic vessel response per degree of freedom. Load RAO relate the amplitude of the incoming wave to the amplitude of the hydrodynamic forces and moments that the wave exerts on the vessel.

For the calculation of the vessel response in OrcaFlex, only one set of load RAO is used. The reason not to use displacement RAO follows from the calculation of the vessel response in OrcaFlex, which is addressed on the next page. The calculation of the load RAO is performed by the hydrodynamic diffraction software ANSYS AQWA. The diffraction theory behind the calculation of the displacement- and load RAO is briefly discussed below, according to (Journée & Massie, 2001). The potential theory and diffraction calculation is described extensively in Appendix B.

In a diffraction calculation, linear potential theory is used to describe the velocity of the water particles due to waves in the fluid field around a floating body (the vessel). For this description, the fluid is assumed to be incompressible to satisfy the mass balance, inviscid to satisfy the momentum balance and, consequently, irrotational. The vessel's total velocity potential is a superposition of the potentials of the undisturbed incoming wave, the diffracted wave due to the fixed body and the (radiation) potential due to the body oscillating in all its degrees of freedom separately:

$$\Phi(x, y, z, t) = \sum_{j=1}^6 \Phi_{r,j}(x, y, z, t) + \Phi_{w,0}(x, y, z, t) + \Phi_{d,7}(x, y, z, t) \quad (2.1)$$

Where:

- $\Phi_{w,0}$ = potential due to the undisturbed incoming wave ($j = 0$) [m^2/s]
- $\Phi_{r,j}$ = radiation potential due to oscillating body motions in all degrees of freedom (for $j = 1..6$) [m^2/s]
- $\Phi_{d,7}$ = potential due to the diffracted undisturbed incoming wave ($j = 7$) [m^2/s]
- x, y, z = coordinates [m]
- t = time in [s]

After applying the kinematic and dynamic boundary conditions, the linearised Bernoulli equation relates the velocity potential of the water particle motion due to waves to the fluid pressure around the vessel. Using linear wave theory (or Airy wave theory) a separation of variables regarding time and space can be made. This leads to:

$$p(x, y, z, t) = -\rho \frac{\partial \Phi}{\partial t} = \rho \omega^2 \left\{ (\phi_0 + \phi_7) \zeta_0 + \sum_{j=1}^6 \phi_j \zeta_j \right\} \cdot e^{-i\omega t} \quad (2.2)$$

Where:

- p = pressure [N/m^2]
- ρ = density of the fluid [kg/m^3]
- ω = wave frequency [rad/s]
- ζ_0 = amplitude of the undisturbed incoming wave [m]
- ζ_j = amplitude of the radiated wave ($j = 1..6$) [m]
- $\phi_{0,7}$ = amplitude of the potential due to the (diffracted) undisturbed incoming wave potential [m]
- ϕ_j = amplitude of the radiation potential due to body motions ($j = 1..6$) [m]

Integrating the pressure over the wetted surface of the hull of the vessel is performed in two steps. The first step is the integration for the contributions of ϕ_0 and ϕ_1 . This results in the first order hydrodynamic wave exciting forces and moments and the phase at which this amplitude occurs. These are the load RAO, which are therefore only dependent on the geometry of the vessel. The integration of the contribution due to the radiation potentials is used to determine the added mass and damping coefficients. Next to the geometry of the vessel, these are dependent on the mass and mass moment of inertia of the vessel and its hydrostatic stiffness.

In order to calculate the vessel response to the environmental conditions, OrcaFlex solves the general equation of motion per time step:

$$(\mathbf{M}+\mathbf{A})\ddot{\underline{x}}(t)+\mathbf{C}\dot{\underline{x}}(t)+\mathbf{K}\underline{x}(t)=\underline{F}(t) \quad (2.3)$$

Where:	\underline{x}	Displacement vector (with respect to its equilibrium position)
	\mathbf{M}	Mass matrix
	\mathbf{A}	Added mass matrix
	\mathbf{C}	Damping matrix
	\mathbf{K}	Stiffness matrix
	\underline{F}	Harmonic wave forces and moments (load RAO) acting on the vessel

As described in Chapter 1, the redistribution of the topside load from the substructure to the vessel is to be performed by the anti-heeling system. Transferring ballast water in the anti-heeling tanks towards portside causes a shift of the Centre of Gravity (CoG) and a corresponding change in the mass moments of inertia of the vessel. Therefore, the values in the mass matrix in equation (2.3) change during the operation. In the OrcaFlex model, this is accounted for by a moving mass. This is discussed in section 2.4, where the anti-heeling system is described. When using displacement RAO, the vessel response would not account for these changes in inertia and thereby the changing natural frequency of the roll of the vessel.

To be fully correct, it should be noted that the hydrodynamic roll and pitch stiffness are subject to minor changes. These depend on the transverse and longitudinal metacentric height (GM_T and GM_L), which are affected by the change of the vertical CoG. However, the main shift of the centre of gravity due to the transfer of the ballast water is in the transverse direction of the vessel, the vertical change of approximately 0.20 meter is not significant. This has a negligible effect on the GM_L , the GM_T is reduced by only less than 2 percent.

Viscous roll damping

As a consequence of the use of potential flow theory, no viscous roll damping is calculated in the diffraction calculation of AQWA. This contribution is calculated beforehand with Safetrans (Boskalis, 2016b), and is added manually in the AQWA input file (per frequency). Safetrans is a frequency domain diffraction solver based on the Tanaka formulation (MARIN, 2016), which uses 2D-strip theory and does account for viscous damping.

2.3. Hoisting system

This section addresses the crane components involved in the OrcaFlex time domain model followed by the operational limits of the hoisting system. A general overview on the nomenclature of a mast crane is given in Figure 2-4.

Inside the pedestal, the drums that store the steel wire ropes for the hoisting systems are located. These drums are connected to winches, which control the length of the wires. Starting from the drums, the wires are going through the crane mast and are guided over the mast head by several sheaves towards specific locations at the

crane boom. A distinction can be made between wires that function in a lifting mechanism (ending at a hoist block) and one wire that has its end fixed to the boom at the location of the main hoist. The latter is the boom hoisting system. In order to have the boom hoisting system stiff enough, the wire is 'coiled' between sheaves on the mast head and at the crane tip multiple times. The number of line elements between the boom and the mast head (in the case of the boom hoist) is called the number of falls. Using the winch of the boom hoist wire allows to vary the luffing angle of the boom with respect to the vessel deck. Together with adjusting the slewing angle, the location of the crane tip can be adjusted until the desired altitude and outreach is met. The other wire ropes are guided over and through the crane boom by sheaves towards their hoisting system and have their other end connected to a hoist block. Two wires end up at the main hoist block, both having multiple falls between the boom and the hoist block.

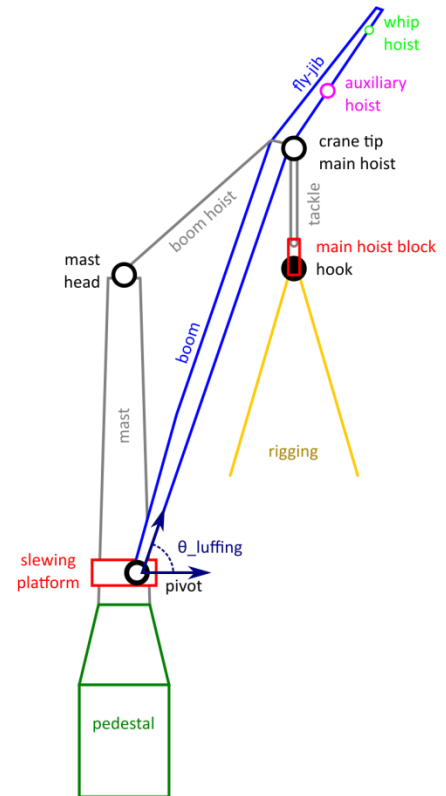


Figure 2-4 Crane nomenclature

Figure 2-5 shows the model of the mast crane, including the pedestal, the slewing platform and the mast for reference only. The rigid bodies (6D Buoy) shown in red are the crane boom and the main hoist block. At the pivot point the boom is constraint such that the only remaining degree of freedom is the luffing rotation. The upper end is kept in place by the boom hoist, shown in light-grey. The dark-grey lines connecting the crane tip to and the main hoist block are the two tackles of the main hoist. Besides being vertically limited in its motions by the tackles, the main hoist block has 6 degrees of freedom. The rigging will be attached to the hook, which is found at the lower end of the main hoist block. The main hoist tackles include a winch, allowing to change their length during a simulation. As the wires from the main hoist and the boom hoist originate from the winches located in the pedestal of the crane, the full wire length should be taken into account regarding their stiffness. In the model however, they are represented by shorter lines with the length of the tackles only. The equivalent axial stiffness (EA) for the full trajectory that the wires follow is used for those lines as this property is nearly constant for small changes in the tackle length.

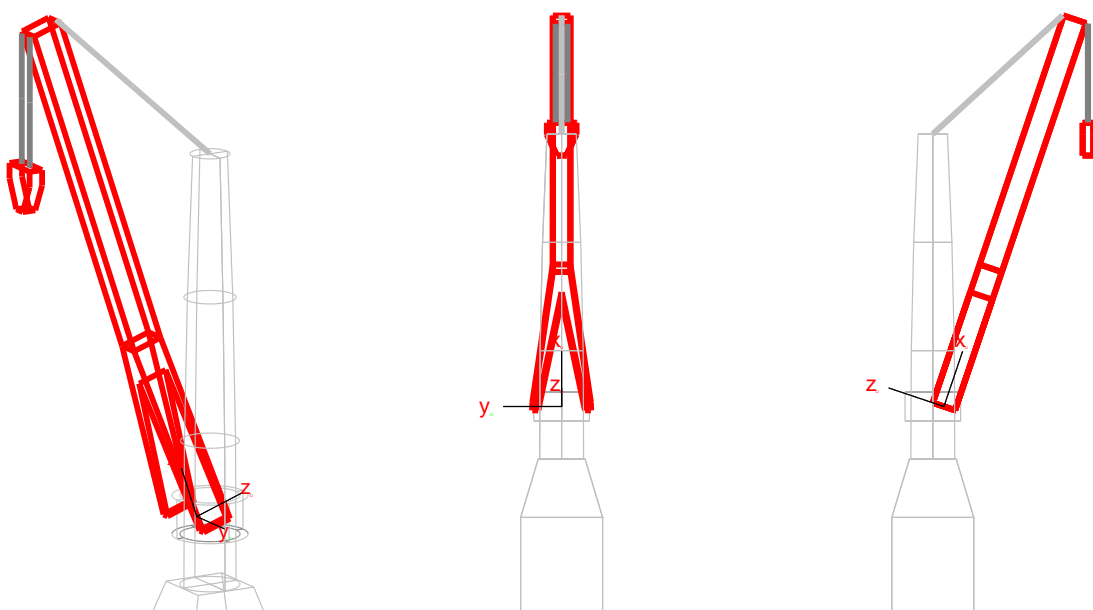


Figure 2-5 Mast crane model

Crane limitations

Next to the lifting capacity of 3,000 tonne the offshore mast crane has other operational limitations. It is designed for operations with a Dynamic Amplitude Factor (DAF) of 1.1. The DAF is the ratio between the highest encountered Dynamic Hook Load (DHL) during an operation and the Static Hook Load (SHL), here consisting of the weight of the topside and the rigging lines. When the hoist block is not located straight below the crane tip a larger moment is applied at the boom and at the pivot point. The horizontal component of the forces on the crane tip, the offlead- and sidelead forces, are therefore limited. The offlead and sidelead angles are the angles with respect to the vertical of the crane mast, shown in Figure 2-6. The limiting horizontal forces correspond with the crane curve for an offlead- or sidelead angle of 2 degrees. As a consequence the maximum heel and trim angle of the vessel are limited to 1 degree. With the sidelead angle also comes a physical limitation, as the outer falls will touch the sheaves at the crane tip when this angle exceeds 4 degrees.

All system limitations are summarised at the end of this chapter.

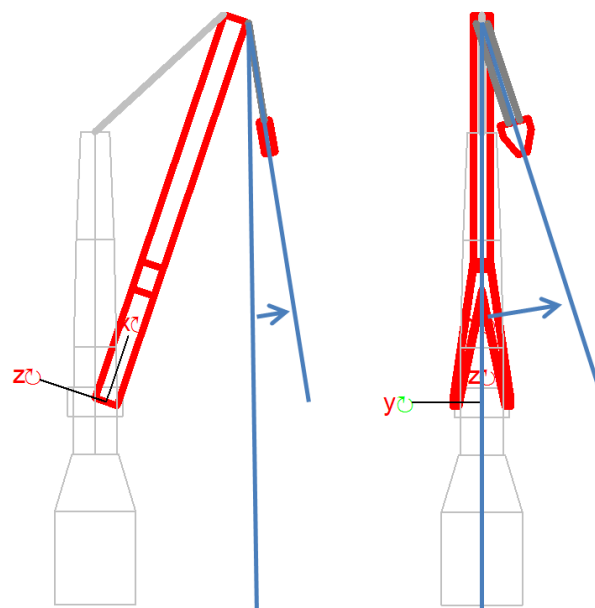


Figure 2-6 Offlead angle (left) and Sidelead angle (right)

2.4. Anti-heeling system

The name of this system directly shows the purpose of it: preventing the vessel from having a heel angle or, stated otherwise, keeping the vessel at even keel conditions. When the tension in the main hoist is increased by decreasing the tackle length, the vessel would not stay within the limit of 1 degree static heel during the decommissioning operation if this was not adjusted for. The anti-heeling system consists of 3 couples of portside and starboard designated water ballast tanks with a total mass of approximately 7,000 tonne. Between the tanks ballast water can be transferred by 8 pumps with a capacity of 2000 m³/hr each. With this system the vessel is able to fully redistribute a 3,000 tonne load within 15 minutes.

As stated in section 1.4.4, the anti-heeling system is used to compensate the heeling moment as the topside is being lifted. With the crane located on the starboard side of the vessel, the ballast water is pumped from starboard to portside in order to create a counter (or anti-heeling-) moment that compensates for the heeling moment caused by the topside mass applied at the crane tip. To be more specific, the anti-heeling system is computer controlled and has two main modes for the redistribution of loads. In the first mode, the manual mode, the pumps are simply switched on in order to provide an anti-heeling moment. The second mode, the

automatic mode, responds to the tension in the hoisting system. When the tackle length is slowly decreased by the winches of the main hoist wires, the tension increases and the vessel will heel. When an increase of tension in the hoisting system is measured the computer will drive the pumps to restore the even keel condition. Regarding the measurement of the tension, this will be an average value over a specific period of time. Therefore a lag of 10 to 30 seconds is present in this mode of the system.

At the start of the decommissioning operation the anti-heeling ballast tanks are filled such that the vessel is at even keel. The CoG of the ballast water applies approximately at the Centre Line (CL) of the vessel, depending on the ballast plan. The heeling moment that is required to lift the topside is obtained at the moment in time when the desired distribution of ballast water is reached. This is illustrated in Figure 2-7.

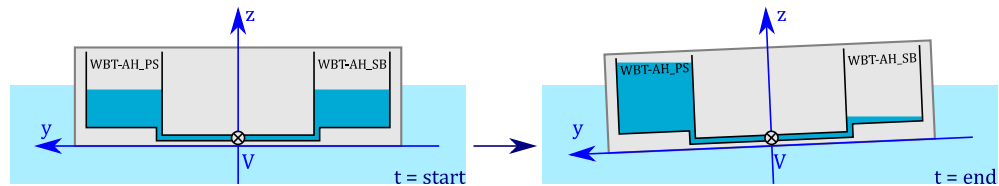


Figure 2-7 Redistribution of ballast water load in designated anti-heeling water ballast tanks

The transfer of ballast water from the starboard to portside tanks is accounted for in OrcaFlex by a 6D Buoy, which has a mass corresponding to mass of the ballast water in both tanks and represents the CoG of the anti-heeling system. The shift of the CoG over time is controlled by two winches, which are shown in black in Figure 2-8. During this shift, the path of the CoG is parabolic. This is accounted for by two shapes, shown in grey, that guide the blue 6D Buoy that represents the mass of the ballast water.

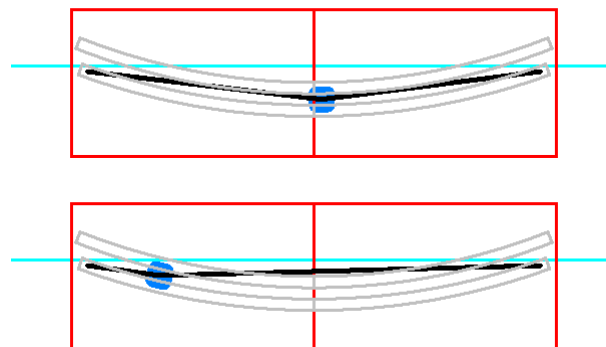


Figure 2-8 Start and end location of the anti-heeling mass

The inertia properties of the vessel system are affected by the moving anti-heeling mass. From the equations of motion for roll, pitch and yaw of the vessel it is clear that the mass moment of inertia affects the natural period and thus the vessel behaviour. As the ballast water is transferred from starboard to portside, the shift of CoG will occur in the vertical y-z plane only, the I_{yy} and thereby the pitch natural period is not affected. In OrcaFlex a local inertia can be given to the 6D Buoy. This represents the local inertia due to the masses in all anti-heeling water ballast tanks. The effect of the shift of this mass on the vessel's inertia will be accounted for by the parallel axis theorem (also known as Steiner's law) shown in equation (2.4), where m is the mass and Δx is the distance of the mass perpendicular to the x-axis of the reference system, which is the vessel's CoG.

$$I_{xx}^{global} = I_{xx}^{local} + I_{xx}^{Steiner} \quad \text{where} \quad I_{xx}^{Steiner} = m \cdot (\Delta x)^2 \quad (2.4)$$

Actually there are two masses with a certain distance to the CL of the vessel. Despite accounting for the shift of the CoG by the 6D Buoy mass the inertia calculation is therefore prone to an error. This is coped with by adding

the difference in inertia to the vessel. The only remark that has to be made regarding the incorporation of the anti-heeling system is that the free-surface effect of the water ballast tanks is neglected.

Based on the installed power of the pumps and the distribution of the water between the portside and starboard tanks, the available head is calculated. For the calculation of the speed of the anti-heeling mass, losses due to skin friction and bends in the pipes that connect two ballast tanks, are accounted for. Some characteristics are presented in the table below.

Table 2-3 Characteristics movement anti-heeling mass

	TCG AH mass [m]	VCG AH mass [m]	flow rate [m ³ /s]	speed AH mass [cm/s]
Equally filled ballast tanks	0.00	5.05	5.18	2.086
End of ballast transfer	13.67	6.62	4.48	1.858

2.5. Horizontal vessel constraints

Limiting the vessels’ second order motions in the horizontal plane during offshore operations will be achieved using a Dynamic Positioning (DP) system or by a traditional catenary mooring system. Both options will be available for the BOKALIFT 1. The class-2 DP system that will be installed meets the recommended DP equipment class for lifting vessels (International Maritime Organisation, 1994). Therefore the DP system is proposed to be used to keep the BOKALIFT 1 at its desired location for the actual decommissioning operations in the future. However using a catenary mooring system is a valid – and the currently most used – option for the operation, modelling-wise it is not an option to replace a DP system. As stated in scope of this thesis, the maximum heeling moment is to be examined. A heavy catenary mooring system limits the symmetric vessel motions more than the DP system due to the vertical component of the tension in the mooring lines as a consequence of their self-weight. Therefore a couple of purely horizontal, massless springs are used to constrain the vessel to its operation location in order not to affect the vessel motions.

An estimation for the spring stiffness of the station keeping system is based on three criteria. First of all, the natural periods of the surge and sway motions should be outside of the wave exciting periods. For these motions, 30 seconds is taken as a lower bound for the natural period. Next to that, the springs should provide enough stiffness to prevent the vessel from large yaw motions. The final criteria is that the forces in the system due to the wave-excited vessel motions are very small compared to the first order wave loads on the vessel. Used are tethers with an axial stiffness of 10,000 kN, a length of 55 meter with an initial elongation of about 1 meter, resulting in a pre-tension of roughly 150 kN. As can be seen in the figure below, the ends are applied at the centre line in order to be sure that the roll motion of the vessel is not affected by the station keeping system.



Figure 2-9 Top view model of horizontal vessel constraints

2.6. Topside and substructure interface

The topside considered is 20 meters in height, covering an area of 25 by 25 meters and weights 2,500 tonne. The size, mass and inertia properties of the topside are provided by Boskalis, as well as the rigging design and the tugger lines. Yawing and pendulum motions of the topside during the lift should be controlled according to (Det

Norske Veritas, 2014a). The guideline recommends to use tugger lines and/or additional bumpers or guides to limit horizontal motions to 1.5 meters, a roll and pitch angle of the topside to 2 degrees and a yaw angle to 3 degrees. Next to that, the minimum clearance between the topside and the crane boom “should normally not be less than 3.0 m”. These criteria are used to determine whether bumpers or guides should be installed next to the tugger lines installed to the crane boom.

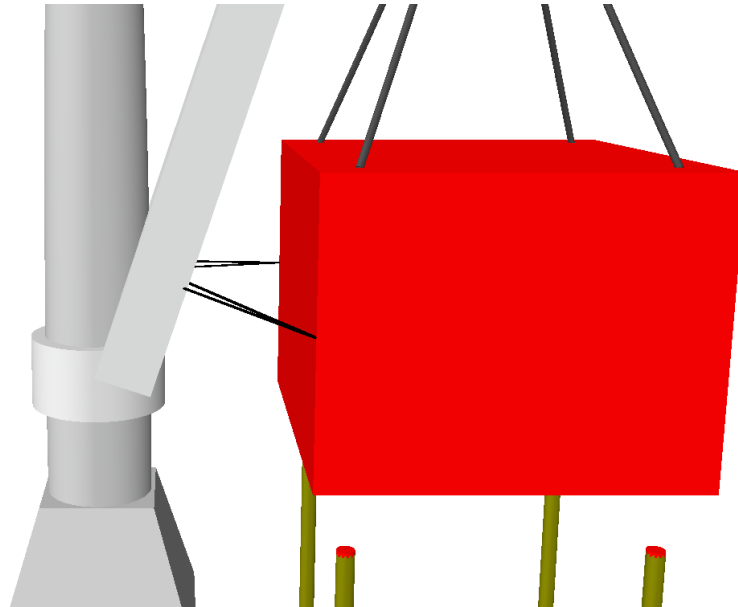


Figure 2-10 Topside model

For the lift simulations two types of leg cuts are investigated, a man-made cut and a machine-made cut, shown in Figure 2-11. In order to have the topside statically supported by the legs after the cutting is performed, the cut types have a certain shape to provide horizontal stability, resisting the topside from sliding off its supports right after the last cut is made. The man-made cut has a conical shape, as the fire torch is held under a certain angle by the man that performs the cut by slowly moving around the leg. For this angle 30 degrees is assumed. For the simulations this cut type is named the Conical cut. The internal cutting tool has more options to cut a shape which can provide horizontal stability. By moving up and down at a predefined interval during rotating in the leg the so-called Carousel cut can be obtained.

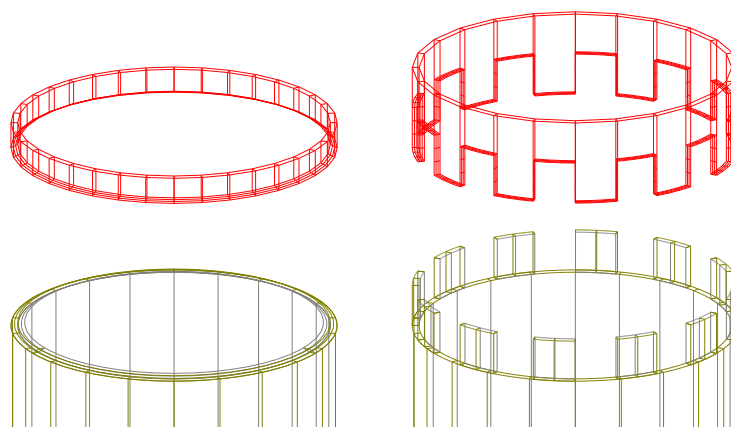


Figure 2-11 Models of the Conical cut (left) and Carousel cut (right)

Contact between two objects can be modelled in OrcaFlex by using shapes and 6D Buoys. The shapes are used to model the lower part of the leg and are fixed to the global axis system. The buoys are used for the upper part and has a fixed connection to the topside, also a 6D Buoy, at a vertical distance of 5 meters. Contact is obtained when multiple edges of a buoy meet the location of the shape, creating a contact area. It is required to have the

full length of these edges in contact with the shape in order to create this area. Therefore, when only the edges on the outer and inner diameter of the pipe are modelled, contact will be lost when with the slightest displacement of the buoy. Therefore a mesh is generated, a part of which can be seen in Figure 2-12. The lower part of the cut, consisting of shapes it is less complicated: standard available shapes are used.

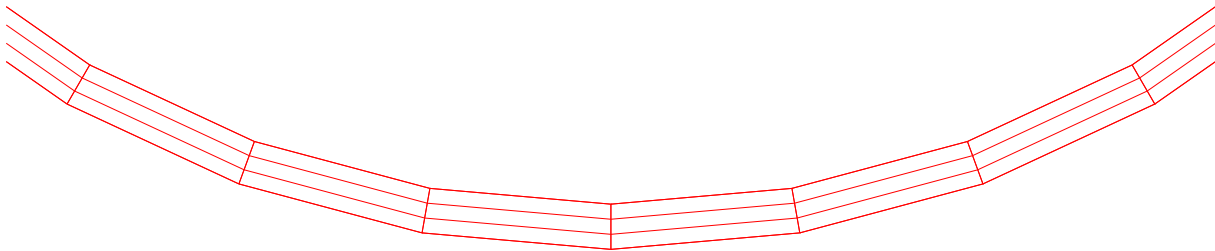


Figure 2-12 Leg cut detail

During the time domain simulation this contact comes along with a friction force. Due to the geometry of the cut this force attributes to the horizontal stability of the supports. OrcaFlex uses a modified Coulomb friction model, in which the friction force is determined by a friction coefficient μ [-] and the contact reaction force R [kN]. A steel to steel friction coefficient of 0.3 is used in accordance with (Det Norske Veritas, 2014b).

2.7. Conclusion

In order to account for all aspects of the dynamically coupled vessel-topside system, all bodies that have degrees of freedom are separated in the model created for the modal analysis and time domain simulations. Next to the vessel also the main hoist block and the topside have 6 degrees of freedom. The 6D Buoys representing the topside and the leg cuts act as one body with 6 degrees of freedom. For the crane boom the luffing rotation at the pivot point is a degree of freedom up to a certain level, as it is constrained by the stiffness of the boom hoist.

The offlead- and sidelead forces and angles are an important aspect of the limitations for the workability of the vessel, also limiting the vessels heel angle. Heeling of the vessel is coped with by the anti-heeling system which is modelled as a single mass that shifts towards portside during the operation. Its location corresponds to the combined CoG of the water in all designated water ballast tanks and its speed is controlled by winches, based on the capacity of the pumps. With the moving anti-heeling mass the vessels inertia properties are subject to change in accordance to reality. Due to the changes in the mass moment of inertia that the movement of the anti-heeling mass implies, displacement RAO are not applicable. The vessel response is calculated by one set of load RAO that provide the hydrodynamic wave loads and the frequency-dependent added mass and damping matrices.

The criteria that limit the workability of the BOKALIFT 1 during the decommissioning operation are listed below.

- Dynamic Amplitude Factor (DAF): 1.1 [-]
- Offlead / Sidelead force: < Max. lifting force * sin (2 degree offlead/sidelead)
- Vessel Heel / Trim angle: < ± 1 degree
- Sidelead angle: < ± 4 degree (physical limit)
- Topside roll and pitch angle: < ± 2 degree
- Topside yaw angle: < ± 3 degree
- Topside motion: < ± 1.5 m horizontal excitation
- Clearance: > 3.0 meter between topside and crane boom

Chapter 3. Modal analysis

This chapter is an assessment to compare the different dynamic configurations described in the problem identification based on a modal analysis. The analysis is performed with OrcaFlex. From this analysis, the coupling between different degrees of freedom and the natural periods of the mode shapes are obtained. The models used contain 3 or 4 rigid bodies with their own degree(s) of freedom, depending on the configuration. Table 3-1 shows the number of degrees of freedom per configuration. The figures of the models used are shown in the next paragraph.

Table 3-1 Degrees of freedom per rigid body per configuration

Configuration:	Uncoupled	Constraint	Coupled
Body:			
Vessel	6	6	6
Crane boom	1	1	1
Main hoist block	6	6	6
Topside	-	-	6
Total	13	13	19

3.1. Mode shapes

The coupling between all degrees of freedom in the mode shapes is expressed in coefficients that are normalised with respect to the largest offset (translation or rotation) of a single degree of freedom, which therefore has a value of 1. Out-of-phase motions have negative values. The tables presented in this paragraph contain the system modes in the columns, which are composed out of contributions from all degrees of freedom, shown in the rows of the tables. Full results for all modes, corresponding to the number of degrees of freedom of the configuration (Table 3-1), are shown in Appendix C.1. Only those of interest are presented here.

3.1.1. Uncoupled and coupled configuration

The title of this section could also have been ‘unconstrained configurations’, as the end of the hoisting system is free to move for both configurations investigated here. In the uncoupled configuration, shown in Figure 3-1, the hoisting system ends at the unloaded, free hanging main hoist block. Figure 3-2 shows the coupled configuration, where the lifted topside is free to move. In both configurations, the hoisting system is able to move as a pendulum, which is hinged at the crane tip.

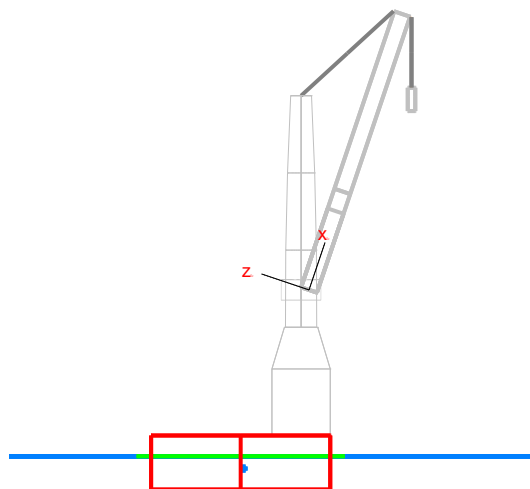


Figure 3-1 Modal analysis: model of the uncoupled configuration

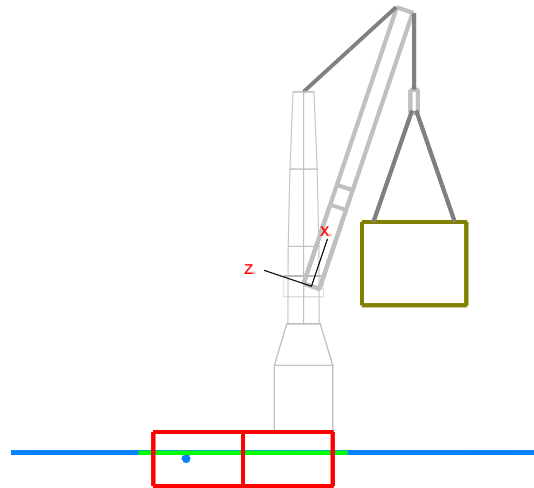


Figure 3-2 Modal analysis: model of the coupled configuration

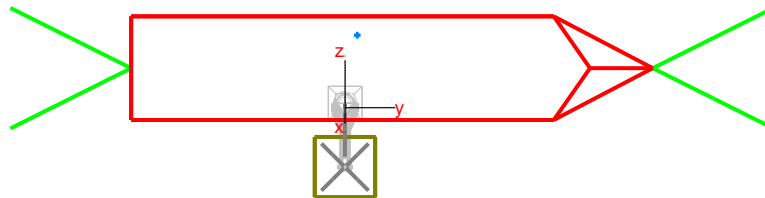


Figure 3-3 Modal analysis: model of the coupled configuration – top view

In Table 3-2 and Table 3-3 the normalised coupling coefficients of the vessel modes are shown for the uncoupled and coupled configuration, respectively. Both show the natural heave-pitch coupling and sway-yaw coupling of the vessel degrees of freedom (Journée & Massie, 2001). The degrees of freedom of the main hoist block in the uncoupled configuration and the topside in the coupled configuration follow the vessel degrees of freedom. As the mass of the main hoist block is small compared to the mass of the vessel, its motions have no influence on the vessel behaviour. This is different for the topside mass, as the last column of Table 3-3 shows. The pendulum motion in the sway direction, or in crane terms, in the offlead direction, counteracts the vessel’s sway motion and, more in particular, the roll motion. The rotational degree of freedom of the crane boom, hinged at the pivot point on the slewing platform and constraint by the stiffness of the boom hoist at the top of the crane tip, does not contribute to any of the vessel modes (as desired).°

Table 3-2 Mode shape coefficients of the uncoupled configuration

Modal analysis 1 - Uncoupled	Vessel mode shapes					
	surge	sway	heave	roll	pitch	yaw
natural period [s]	59.47	115.55	4.83	11.97	5.44	55.01
Vessel; X (m)	0.993	0.000	-0.071	0.000	0.130	-0.014
Vessel; Y (m)	0.049	0.963	0.011	-0.027	-0.029	1.000
Vessel; Z (m)	0.001	0.000	0.997	0.001	-0.589	0.000
Vessel; RX (deg)	0.000	-0.005	0.012	-0.115	-0.066	-0.001
Vessel; RY (deg)	0.000	0.000	0.363	0.000	-0.661	0.000
Vessel; RZ (deg)	-0.026	0.013	-0.005	0.001	0.008	-0.518
HoistBlock; X (m)	1.000	0.009	-0.243	0.003	0.624	-0.379
HoistBlock; Y (m)	0.010	1.000	0.005	0.573	-0.055	0.207
HoistBlock; Z (m)	0.000	0.004	0.430	0.080	0.483	0.001
HoistBlock; RX (deg)	0.001	0.017	0.087	1.000	-0.697	0.016
HoistBlock; RY (deg)	0.000	0.000	0.390	0.000	-0.717	0.000
HoistBlock; RZ (deg)	-0.027	0.013	0.001	0.002	-0.002	-0.553
BoomConstraint; RY (deg)	0.000	0.000	-0.004	-0.002	-0.006	0.000

Table 3-3 Mode shape coefficients of the coupled configuration

Modal Analysis 3 - Coupled	Vessel mode shapes						Topside
	surge	sway	heave	roll	pitch	yaw	sway
natural period [s]	61.09	118.73	4.96	10.27	5.49	56.48	28.40
Vessel; X (m)	0.912	0.000	-0.079	0.001	-0.095	0.012	-0.001
Vessel; Y (m)	-0.033	0.921	0.020	0.046	0.018	1.000	-0.194
Vessel; Z (m)	0.002	0.000	0.997	-0.003	0.324	-0.001	0.001
Vessel; RX (deg)	0.001	-0.025	0.039	0.385	0.024	-0.019	-0.382
Vessel; RY (deg)	0.001	0.000	0.385	-0.001	0.467	0.000	0.000
Vessel; RZ (deg)	0.018	0.005	-0.007	0.007	-0.007	-0.528	0.031
Topside; X (m)	1.000	0.004	-0.071	-0.002	-0.106	-0.401	0.033
Topside; Y (m)	-0.008	1.000	0.005	0.433	0.008	0.244	0.960
Topside; Z (m)	0.000	0.018	0.398	-0.280	-0.438	0.014	0.279
Topside; RX (deg)	0.000	0.016	0.057	1.000	0.075	0.018	0.276
Topside; RY (deg)	-0.061	0.000	0.860	0.005	0.997	0.029	-0.009
Topside; RZ (deg)	-0.013	0.015	0.000	0.000	0.000	0.294	-0.003
HoistBlock; X (m)	0.949	0.004	0.642	0.002	0.724	-0.378	0.025
HoistBlock; Y (m)	-0.007	0.986	-0.042	-0.415	-0.055	0.229	0.724
HoistBlock; Z (m)	0.000	0.018	0.392	-0.279	-0.433	0.014	0.278
HoistBlock; RX (deg)	0.000	0.016	0.025	0.868	0.040	0.018	0.272
HoistBlock; RY (deg)	-0.028	0.000	0.377	0.001	0.499	0.013	-0.004
HoistBlock; RZ (deg)	-0.009	0.014	-0.001	0.001	-0.001	0.190	0.001
BoomConstraint; RY (deg)	0.000	-0.001	-0.020	0.002	0.020	-0.001	-0.010

3.1.2. Constraint configuration

For the constraint configuration (see Figure 3-4), the topside is set to be fixed to the global axis system. The topside is hidden in the figures, in order not to give the impression that it could move. Thereby, the lower ends of the rigging lines are fixed. These positions corresponds to the connection points at the topside. The tension in the rigging lines constrain the displacement of the hoist block at the hook. On its turn, the tension in the main hoist tackles constrain the motions of the crane tip. Thereby, excitations of the vessel in all its degrees of freedom are affected and will show therefore more coupling with other degrees of freedom than in the previous cases.

The constraint system is evaluated for two points in time during the decommissioning operation: in a pre-tensioned condition (the left model in Figure 3-4) and right before the transient lift phase (the model shown on the right). Between those phases, the tension in the hoisting system is increased by a reduction of the tackle length and the shift of the anti-heeling mass towards portside. The coupling increases due to increase of tension in the hoisting system, but no difference is seen in the contributing degrees of freedom per mode shape. Therefore, only the normalised coupling coefficients of the latter condition is presented in Table 3-4.

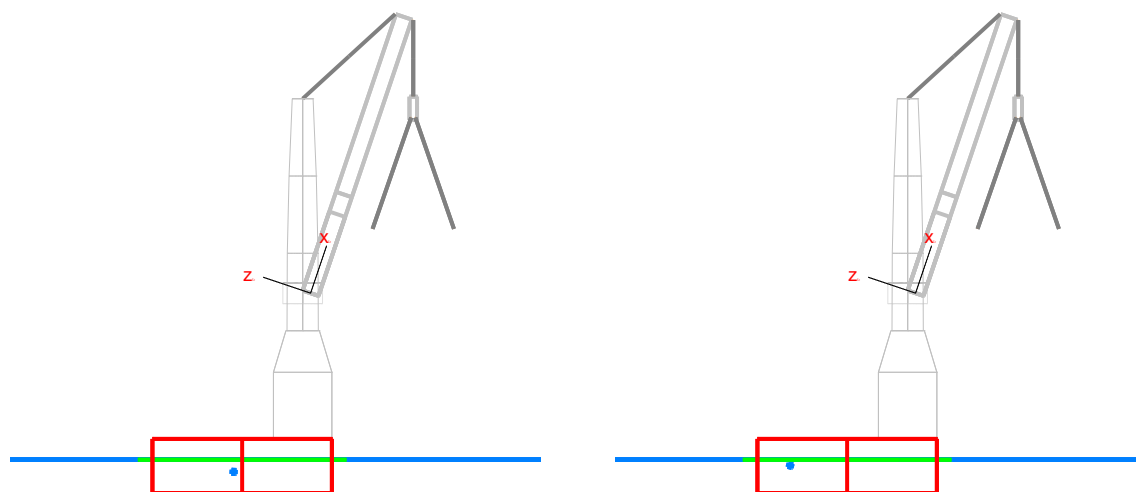


Figure 3-4 Modal analysis: model of the constraint configuration

Table 3-4 Vessel mode shape coefficients of the constraint configuration

Modal analysis 2b - Constraint (lift conditions)	Vessel mode shapes					
	surge	sway	heave	roll	pitch	yaw
natural period [s]	39.85	61.36	5.02	1.84	5.66	27.27
Vessel; X (m)	0.279	0.482	-0.054	-0.006	0.012	-0.415
Vessel; Y (m)	0.904	0.876	0.036	-0.083	0.050	0.908
Vessel; Z (m)	0.022	-0.008	0.620	0.139	0.087	0.053
Vessel; RX (deg)	0.048	-0.013	0.242	-0.425	0.313	0.028
Vessel; RY (deg)	0.001	-0.001	0.306	0.031	-0.071	0.025
Vessel; RZ (deg)	-0.167	-0.675	0.004	0.000	0.002	-0.421
HoistBlock; X (m)	0.011	0.000	0.042	0.004	-0.010	-0.043
HoistBlock; Y (m)	0.053	-0.014	-0.041	0.053	-0.053	0.019
HoistBlock; Z (m)	-0.006	0.001	-0.006	0.111	-0.006	-0.002
HoistBlock; RX (deg)	-0.989	0.254	0.759	-0.997	0.989	-0.363
HoistBlock; RY (deg)	0.143	-0.003	0.651	0.072	-0.150	-0.578
HoistBlock; RZ (deg)	-0.022	-0.085	0.001	-0.001	0.001	-0.054
BoomConstraint; RY (deg)	0.002	-0.001	-0.020	0.231	-0.022	0.001

The negligible coupling terms of the translational degrees of freedom of the hoist block for the vessel mode shapes confirm the constrain at the hook. The hoisting wires connecting the main hoist block and the crane tip can be seen as a semi-rigid bar which is hinged at both ends. The lower hinge of this bar can be considered fixed. Consequently, the crane tip can only move in the horizontal plane. A horizontal displacement of the crane tip causes a rotation of the bar, resulting in horizontal components in the connection force with the hoisting system, the offlead and sidelead forces. When the vessel is excited in the surge and sway degrees of freedom these forces apply a yawing moment due to the misalignment of the longitudinal location of the crane tip and the vessels longitudinal centre of gravity. Therefore all anti-symmetric vessel modes are coupled.

The same principle applies for the heave degree of freedom of the vessel where the vertical component of the tension at the crane tip creates a moment with respect to the centre of gravity of the vessel, coupling it significantly to the roll and pitch degrees of freedom. Figure 3-5 shows the (exaggerated) displacements about the vessel’s mean position for the excitation of the heave mode of the vessel, from which the roll and pitch coupling can be seen. The mode shapes for the other vessel modes can be found in Appendix C.1. Due to the shift of the centre of rotation to the hook, also the pitch mode is coupled to the roll degree of freedom. The roll mode shape itself is the only mode shape that excites the luffing ability of the boom hoist.

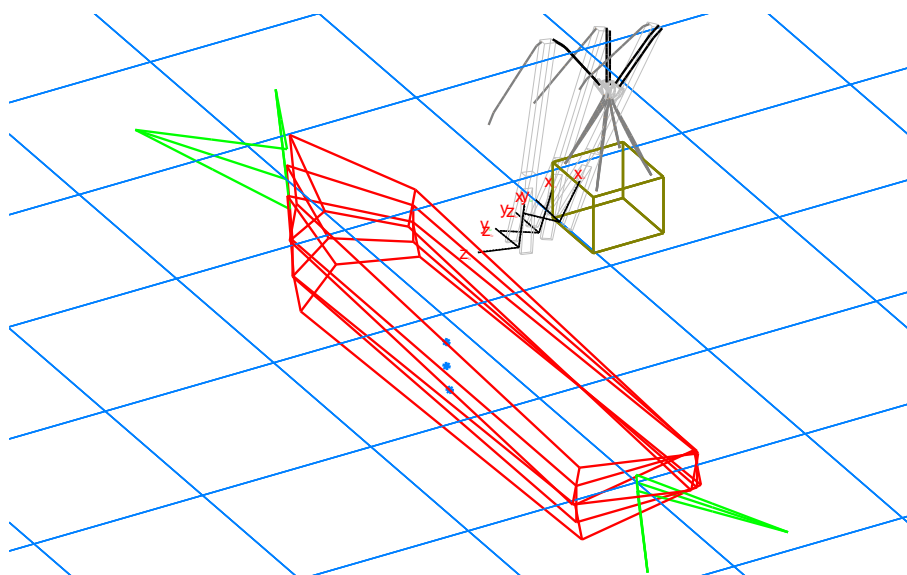


Figure 3-5 Vessel heave mode – constraint model

3.2. Natural periods

Each mode shapes has a natural or fundamental period. OrcaFlex calculates the mode shapes for a multibody system purely based on the vessels hydrostatic properties and the stiffness of the constraints attached to it. Therefore the undamped natural periods presented in the following figures do not include the frequency-dependent added mass.

The increase in stiffness of the system due to the constraint at the crane tip reduces the natural periods of the anti-symmetric motions, which are shown in Figure 3-6 for all investigated configurations. Between the two free floating conditions a small increase in the natural periods is observed. This is caused by the topside mass applied at the crane tip, which increases the inertia of the system. The increase in tension in the hoisting system between the pre-tensioned and lift phase increases the stiffness the system. Hereby the natural periods decrease between the two analyses performed for the constraint configuration.

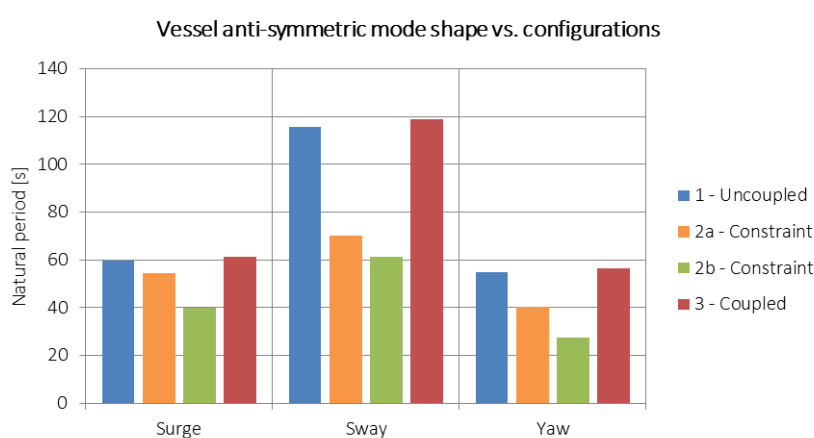


Figure 3-6 Undamped natural periods of the anti-symmetric vessel modes

The natural period of the roll mode of the vessel experiences the largest influence of the stiff constrain on the vertical motions of the crane tip, as can be seen from Figure 3-7. In contrast to the anti-symmetric modes the natural period of the roll mode decreases between the two unconstraint configurations. This is due to the anti-phase coupling of the topside sway mode with the roll degree of freedom.

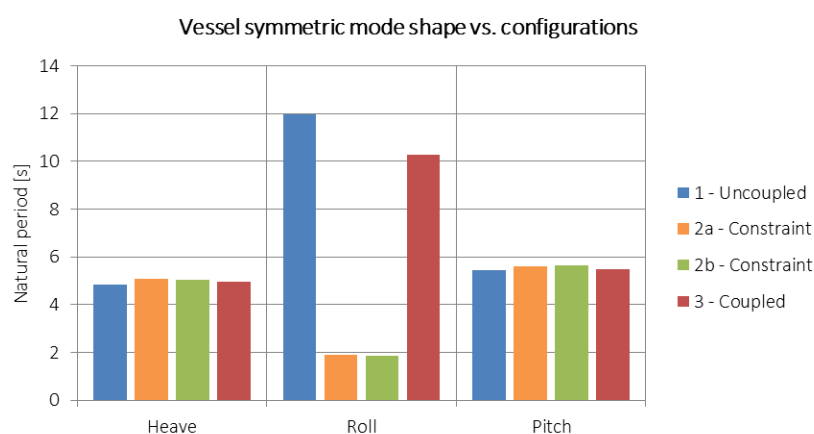


Figure 3-7 Undamped natural periods of the symmetric vessel modes

In the time domain simulations described in the next chapter different sea states are investigated. Therefore it is important to examine the correct natural periods of the vessel in order to identify resonance periods. Including the frequency dependent added mass the undamped natural periods of the symmetric vessel modes become:

Table 3-5 Natural periods symmetric vessel motions including added mass

Natural period [s]	heave	roll	pitch
Uncoupled	8.59	14.20	8.56
Constraint (pre-tensioning phase)	8.97	2.20	8.86
Constraint (lift phase)	8.88	2.14	8.92
Coupled	8.82	12.02	8.64

3.3. Conclusion

The most important findings of the modal analysis of the different configurations are listed below.

- Adding a constrain by tensioning the hoisting system couples all anti-symmetric vessel motions
- The change of the natural roll period of the vessel will cross the wave loading periods during the transient pre-tensioning and lift phases
- The anti-phase coupling of the topside pendulum motion in transverse direction of the vessel with the roll degree of freedom of the vessel slightly reduces the natural period of the vessel roll mode compared to its free floating conditions.
- The natural periods of the heave and pitch modes of the vessel are not significantly affected by the constrain at the crane tip, however strong coupling with the roll degree of freedom is introduced.

Regarding the set-up of the time domain simulations, wave periods corresponding to the natural periods of the vessel modes should be included. The lower bound is set at 2.2 seconds according to the vessel roll mode in constraint conditions. As long as the limiting workability criteria listed in paragraph 2.7 are not exceeded, the upper bound is set by the natural period of the roll mode of the vessel in coupled conditions, at 12 seconds. In between the vessel response for wave periods of 8 and 9 seconds is of particular interest due to the natural periods of the heave and the pitch modes through all configurations.

Chapter 4. Tension variation and set-up of transient time-domain simulations

As stated in the methodology, time-domain simulations are performed in order to identify the amplitude of the tension variation and the vessel behaviour during the transient pre-tensioning and lift phases of the decommissioning operation. Before the different set-ups for the transient time-domain simulations are discussed, the environmental conditions are defined. As the simulation conditions of the transient pre-tensioning and lift phases depend on the amplitude of the tension variation, the results on the tension variation are presented in this chapter. For the simulations, the wave periods investigated are chosen in correspondence with the results of the modal analysis.

4.1. Environmental conditions

As stated in the introduction the BOKALIFT 1 will operate mainly in the North Sea, where many decommissioning operations are to be performed the coming years. A water depth of 100 meters is used, based on the UK sector of the North Sea (see Figure 4-1). For this location a JONSWAP wave spectrum applies. Accordingly, the spectral enhancement factor (γ) is set to 3.3 [-] (Det Norske Veritas, 2007). For each simulation a different random sea state is generated.

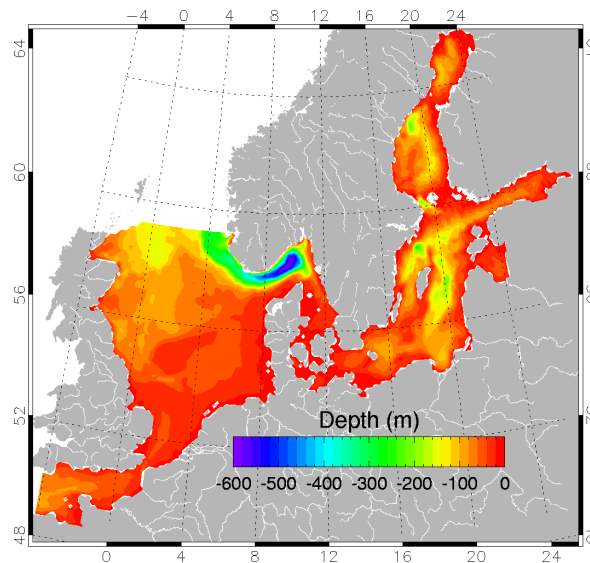


Figure 4-1 Water depth North Sea (Danish Meteorological Institute, 2016)

In order to limit the vessels roll motion, the decommissioning operation is preferably performed in head waves. Wave directions (hereafter indicated by θ) of 180 and 210 degree are investigated.

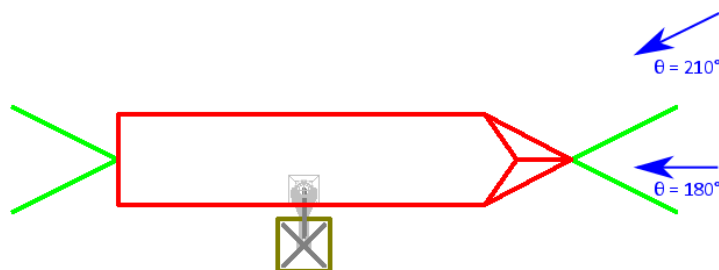


Figure 4-2 Wave directions

In correspondence with the lower and upper bounds set by the natural periods of the vessels roll mode shapes, simulations with peak periods ranging from 2.2 to 12 seconds are performed. Due to wave steepness, the maximum significant wave height (H_s) for wind waves depends on the peak period (T_p). According to (Det Norske Veritas, 2016) the following applies for areas where swell is significant:

$$\sqrt{12.4H_s} \leq T_p \leq 18.2 \quad \text{for} \quad H_s \leq 5.7 \text{ m} \quad (3.1)$$

Initial simulations showed that for a significant wave height higher than 3 meter the crane limits are exceeded and is therefore taken as upper limit. This leads to the following maximum significant wave heights used:

Table 4-1 Sea states

T_p [s]	2.2	3	4	5	≥ 6
H_s [m]	0.5	1.0	1.5	2.5	3.0

For heavy lift operations the guidelines (Det Norske Veritas, 2014a) recommend to perform the operation for sea states with a maximum significant wave height of 2.0 meters. Therefore, additional simulations are performed with this significant wave height for sea states with a peak period of 5 seconds or longer.

Wind and current loads are not included in the simulations. These are considered to be static loads during the short pre-tensioning and lift simulations.

4.2. Even keel conditions

Before the simulations regarding the tension variation can be set, the tension level for which the rigging is pre-tensioned is estimated by static calculations. The system is defined to be pre-tensioned when the rigging lines are taut. This is the case when the elongation of the lines and hoisting wires is linear for an increase of the tension level, according to Hooke’s law. The variation of the tension due to the wave-excited vessel motions raises the pre-tension level.

As the vessel is supposed to perform the operation in even-keel conditions the anti-heeling system is involved in this calculation as well. Figure 4-3 shows the relation between the tackle length and the location of the anti-heeling mass (AH-location). The origin of this location is defined as the mass corresponds to the centre line of the vessel. For a location of 100% the maximum anti-heeling moment is applied. The counter moment created by a shift of the anti-heeling mass of 10% increases the tension in the main hoist with approximately 10% of the topside weight. This relation is linear, as by Hooke’s law.

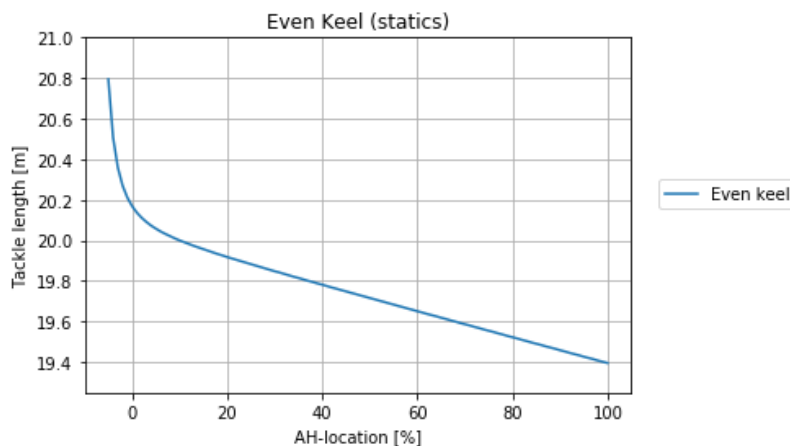


Figure 4-3 Tackle length versus anti-heeling mass location for even-keel conditions

According to the relation between the tension in the hoisting system and the tackle length shown in Figure 4-4, the system is pre-tensioned in static conditions for a tackle length of 20.00 m. This corresponds with a tension in the main hoist of 6550 kN, which includes the weight of the rigging lines and the main hoist block. With a guestimate of the amplitude of the tension variation of 2450 kN in the worst case (10% of the topside weight), the lower bound for the actual calculations of the tension variation is set at 9100 kN, corresponding with a tackle length of 19.91 meters and the anti-heeling system operating at 20% of its maximum capacity.

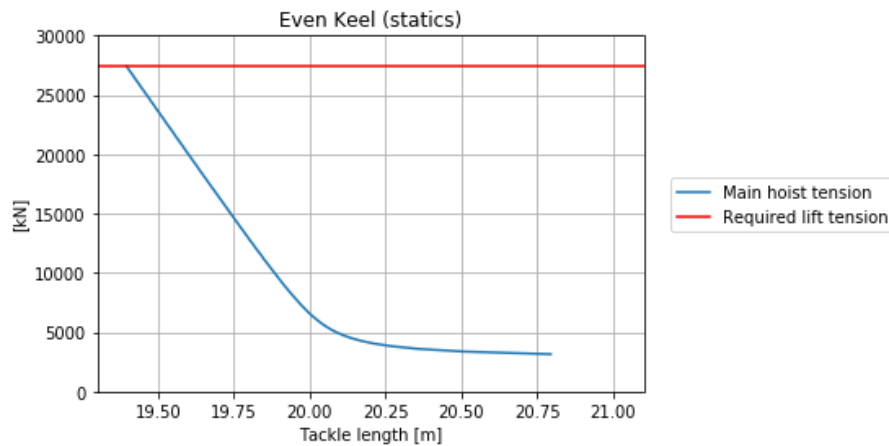


Figure 4-4 Main hoist tension versus tackle length for even-keel conditions

4.3. Tension variation and workability

In order to examine the workability of the vessel and the amplitude of the tension variation, time domain simulations with a duration of 3 hours are performed. Based on the number of wave excitations during this simulation the maximum system response is a good estimate for the most probable maximum values (Det Norske Veritas, 2007). The OrcaFlex model for the constraint configuration is used for these simulations.

A workability study is performed to determine the maximum allowable significant wave height per peak period. The workability criteria listed in paragraph 2.7 are checked for simulations with sea states up to a significant wave height of 3.0 meters. Hereby the significant wave height is lowered in steps of 0.5 meters if at least one of the criteria is exceeded. To evaluate the maximum criteria, the conditions of the constraint model used matches the vessels characteristics of the lift phase. Here, the anti-heeling system provides the maximum counter moment and the tackle length corresponds to even-keel conditions. As the system would actually be in the transient lift phase for these conditions the system would no longer be fully constraint, which makes this analysis conservative. This results in the maximum significant wave heights per peak period presented in the table below, which are used for the following tension variation, pre-tensioning and lift simulations. The limiting criteria are the offlead and sidelead forces due to the horizontal crane tip motions.

Table 4-2 Maximum significant wave height (H_s in [m]) per peak period

T_p [s]	2.2	3	4	5	6	7	8	9	10	11	12
$\theta=180$ [deg]	0.5	1.0	1.5	2.5	3.0	3.0	3.0	2.5	2.0	1.5	1.5
$\theta=210$ [deg]	0.5	1.0	1.5	2.5	3.0	3.0	3.0	2.0	2.0	1.0	1.0

The maximum tension in the main hoisting system found in the workability analysis is used to define the transient lift phase. Subtracting the static hook load due to the weight of the topside, rigging and the main hoist block results in the maximum amplitude of the tension variation at the crane tip per sea state. These are shown in Table 4-3, where the significant wave used corresponds with the maximum value found in Table 4-2. The

guestimate that the maximum amplitude of the tension variation is approximately 10% of the topside weight made in the previous section proves to be a good initial estimation here.

Table 4-3 Maximum amplitude of the tension variation [kN] - Lift phase

Tp [s]	2.2	3	4	5	6	7	8	9	10	11	12
θ=180 [deg]	1206	2407	1781	2009	1825	1523	1365	1198	1107	1604	1957
θ=210 [deg]	928	1700	1590	1971	1535	1835	2253	1388	1457	1669	2247

Determining the tension variation regarding the pre-tensioning simulations is based on the conditions set in the previous paragraph, where 20% of the counter moment is provided by the anti-heeling system. The amplitude in pre-tensioned conditions is based on the *minimum* tension in the hoisting system found from the 3 hour simulations. Subtracting this from the static tension level in these conditions results in the values presented in the table below. Again, the significant wave height used corresponds with the maximum value found in Table 4-2. As the guestimate used is not exceeded, the operating conditions with the anti-heeling mass at 20% is safe for all sea states.

Table 4-4 Maximum amplitude of the tension variation [kN] – Pre-tensioning phase

Tp [s]	2.2	3	4	5	6	7	8	9	10	11	12
θ=180 [deg]	370	1971	1751	1850	1883	1405	1602	1227	815	456	588
θ=210 [deg]	333	2122	1462	1793	1798	1409	1476	957	719	569	645

When the snap loading of the rigging is overcome and the hoisting system is pre-tensioned, the topside legs are cut one by one. During the cutting of a leg the mean tension in the hoisting system is kept constant. In order to fully cover the workability of the vessel between the pre-tensioning and lift phases, three intermediate tension levels are investigated. These correspond with counter moments applied by the anti-heeling system at 40, 60 and 80 percent of its capacity. In general, the largest tension variation occurs at the start and at the end of the constraint configuration, thus right after the pre-tensioning phase and just before the lift phase. The intermediate cases investigated result in lower values for the tension variation. Therefore, no hazardous situations are expected to occur during the cutting process. The maximum amplitudes encountered in these simulations are provided in Appendix C.

4.4. Pre-tensioning the hoisting system

The models for the modal analysis and the tension variation simulations used so far did not change in time. This is different for the pre-tensioning (and the lift) simulations, where the tackle length of the main hoist is decreased and the anti-heeling mass providing the counter moment is moving. In the pre-tensioning phase the rigging lines are going from a slack to a taut condition, during which snap loads are experienced. The amplitude of the snap loads that occur during this phase depend on the initial velocity of the main hoist block. During the first 20% of the load redistribution the snap loads are expected according to the amplitude of the tension variation of the dynamic hook load.

Two schemes for the pre-tensioning of the rigging lines are evaluated. For both pre-tensioning schemes, simulation are performed for all sea states presented in Table 4-2. Next to that sea states with a significant wave height of 2.0 meter are investigated. As these are short simulations, multiple simulations containing different, random wave components need to be performed per sea state in order to investigate the range of maximum amplitudes in the dynamic hook load due to the snap loads.

Regular

For the first pre-tensioning scheme, the manual mode of the anti-heeling system is used. This implies that the anti-heeling moment is continuously increases during the pre-tensioning. Correspondingly the tackle length is decreased such that even-keel conditions are met throughout the full simulation. An even-keel condition is desired during the operation to limit the offlead and sidelead angles and forces. The left graph in Figure 4-5 shows the relation in time.

As soon as possible (ASAP)

The other pre-tensioning scheme simulates the automatic mode of the anti-heeling system, which responds to changes in the average tension in the hoisting system. Therefore these simulations start with decreasing the tackle length. In order to obtain a quick response of the anti-heeling system, the tackle length is decreased as soon as possible by applying the maximum speed of the winches of the main hoist wires (see Figure 4-5). This higher lifting speed of the main hoist is expected to result in a higher amplitude of the snap loads, as the relative velocity of the crane hook is higher than for the regular pre-tensioning scheme. Next to that, the vessel motions are expected to be constrained earlier.

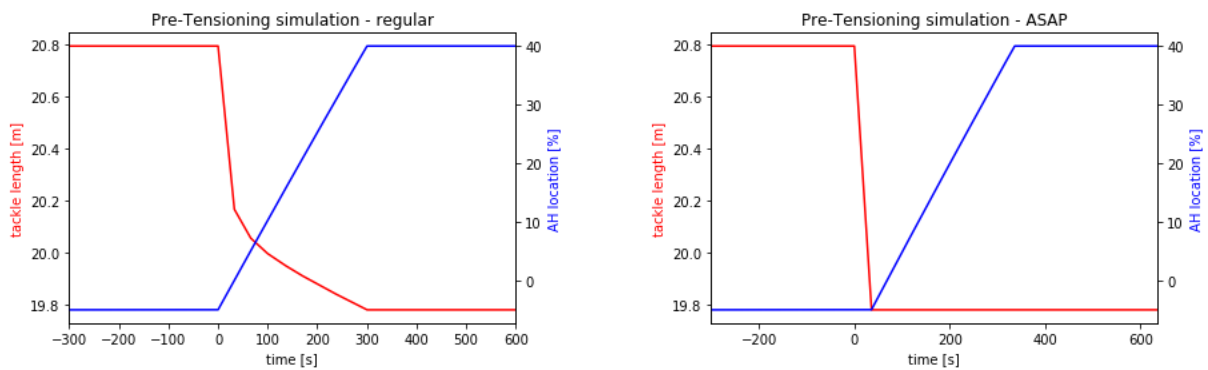


Figure 4-5 Pre-tensioning schemes

4.5. Lift of the topside

After cutting the last leg and the transfer of personnel and equipment, the topside is to be lifted. As there is no longer a physical connection between the topside and its supporting substructure the tension in the main hoist should be significant. The speed of the redistribution of the topside load to the hoisting system is driven by the capacity of the anti-heeling system. During the last 10% of the load redistribution the impact loads are expected to occur, according to the tension variation simulations. Again, two lifting schemes are evaluated.

Regular

Like in the regular pre-tensioning simulations, the vessel is kept at even-keel conditions during the full lift operation in the first lifting scheme. This results in the largest operation window regarding the crane offlead and sidelead forces. Until the anti-heeling system provides the maximum counter moment, the decreasing tackle length compensates the elongation due to the increase in tension. When the required lift tension in the hoisting system is obtained, the topside is lifted at the maximum speed of the winches of the main hoist.

As soon as possible (ASAP)

The start of this lifting scheme is the same as the regular lifting scheme, where the even-keel conditions are maintained. A reduction of the number of impact loads is attempted here by increasing the lift speed at the start of the transient lift phase, thus when the anti-heeling system provides 90% of its counter moment.

Evaluation lifting schemes and type of leg cut

For the regular lift scheme the sea states with a peak period from 2.2 to 9 seconds are evaluated according to Table 4-2. Also the peak period corresponding to the natural roll period of the vessel in the coupled configuration is investigated. Next to these, simulations with the recommended maximum significant wave height for the operation (2.0 meter) are performed. The different lifting schemes as well as the influence of the leg cut types are compared for the sea state with a peak period of 7 seconds in order not to have the results influenced by the natural heave and pitch period. Both the man-made conical shaped cut and the machine-made carousel cut are used in combination with the regular lifting scheme. As these are short simulations, multiple simulations per sea state are performed in order to investigate the behaviour of the topside and the crane loads during the lift operation.

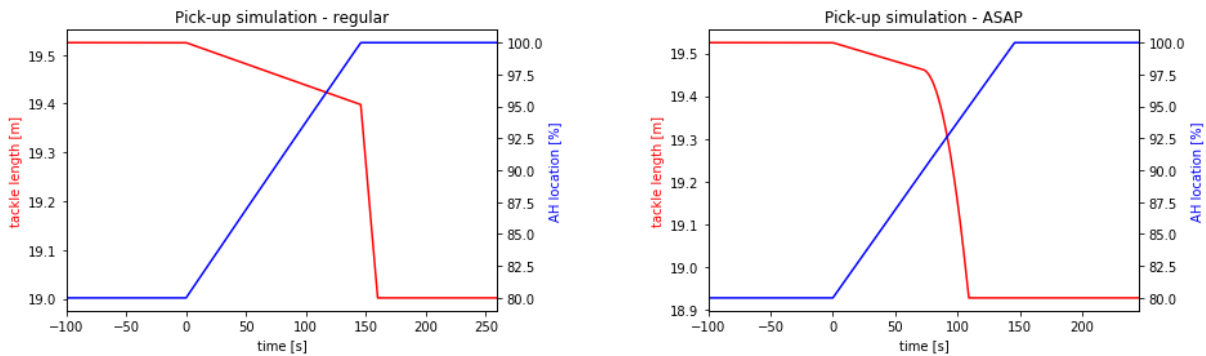


Figure 4-6 Hoisting schemes for the lift phase

Chapter 5. Results transient time-domain simulations

This chapter discusses the results of the time domain simulations of the transient pre-tensioning and lift phases, respectively. The results for all sea states investigated are provided in Appendix C.

5.1. Pre-tensioning simulations

Due to the snap loads that occur in the rigging lines during the pre-tensioning phase, a large variation in tension in the hoisting system is found. As multiple simulations per sea state are performed, the simulations presented here resulted in an average value of the amplitude of the tension peaks. A discussion on the mean and maximum values found is given at the end of this paragraph. Consistently the results for pre-tensioning scheme where the maximum hoist speed is applied (ASAP pre-tensioning scheme) are shown in the graphs on the right on the next page.

The amplitude of the dynamic tension in the hoisting system, the dynamic hook load (DHL), is evaluated with respect to the increasing mean hook load in time. This mean, 'static' hook load (SHL) is determined from a time domain simulation where no waves are present. The dynamic tension in the hoisting system is shown in Figure 5-1. Static calculations have shown that for a static hook load of 6550 kN the rigging lines are taut. For the ASAP pre-tensioning scheme, the desired tackle length is obtained earlier due to the higher hoisting speed. However, by reducing the tackle length only, the desired static hook load is not yet obtained. The counter moment applied by the anti-heeling system is therefore needed to obtain the tension for which the rigging lines are taut.

Due to the higher hoisting speed applied in the ASAP pre-tensioning scheme, the snap loads can start to occur earlier. However, this also depends on the phase of the vertical motion of the crane hook, shown in Figure 5-2, as the snap loads occur for an upwards motion of the hook. Figure 5-3 shows the vertical velocity of the crane tip and the hook. Initially the hook has a higher velocity than the crane tip due to the hoisting speed, which is no longer the case when the snap loads are present and the system is in transition between the uncoupled and constraint configuration. In this transition, the vessel searches for a new equilibrium, as its motions become constrained and the centre of rotation shifts to the hook. The first snap loads quickly decelerate the vertical hook and crane tip motions, thereby increasing the amplitude of the velocity. Consequently the amplitude of the peaks in the dynamic hook load increase. Therefore the largest snap load is not the first that is encountered. Due to the higher hoisting speed, this is most significant for the ASAP pre-tensioning scheme.

Figure 5-4 shows the roll motion of the vessel, showing the even-keel condition of the vessel for the regular pre-tensioning scheme. As the anti-heeling system only starts to respond after reducing the tackle length as soon as possible in the other scheme, this condition is not met. This results in a maximum heel angle of 0.5 degree, half of the maximum allowed heeling angle during the operation. Interesting to see is the difference between the periods of the roll motion of the vessel and the vertical motion of the crane tip (shown in Figure 5-3). The latter matches the natural period of the vessel roll mode found for the constraint configuration, but this does not affect the period at which the vessel rolls. According to the modal analysis the heave and pitch modes are coupled to the roll degree of freedom due to the constraint, which shows to be dictating the roll behaviour of the vessel during these conditions.

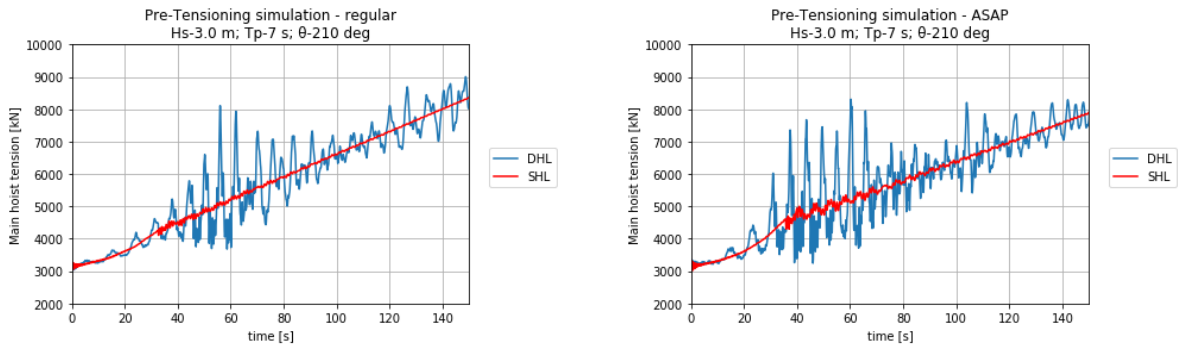


Figure 5-1 Main hoist tension

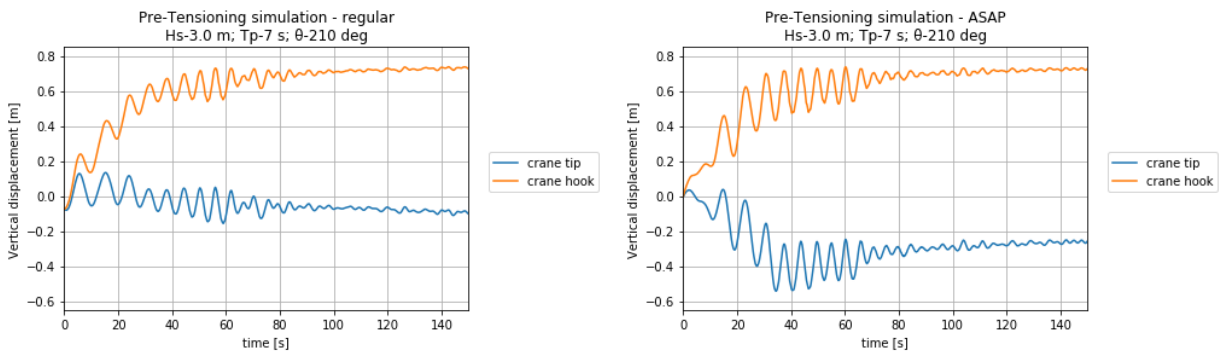


Figure 5-2 Vertical motions of the crane tip and crane hook

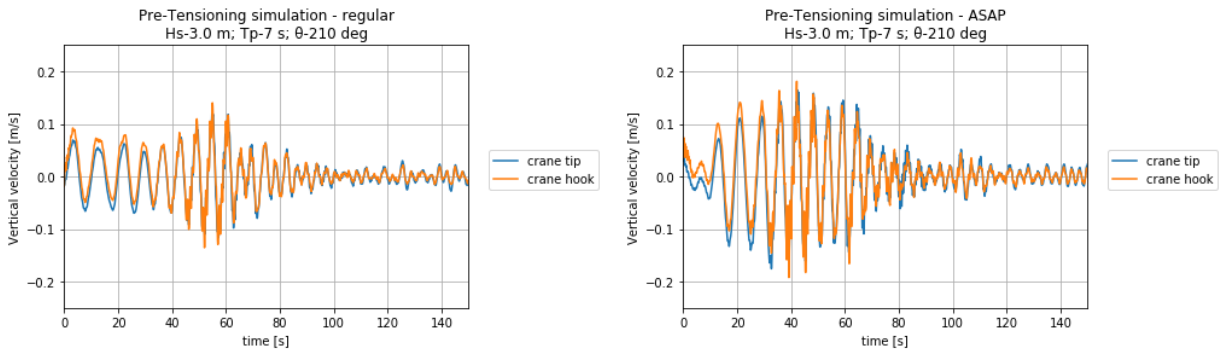


Figure 5-3 Vertical velocity of the crane tip and crane hook

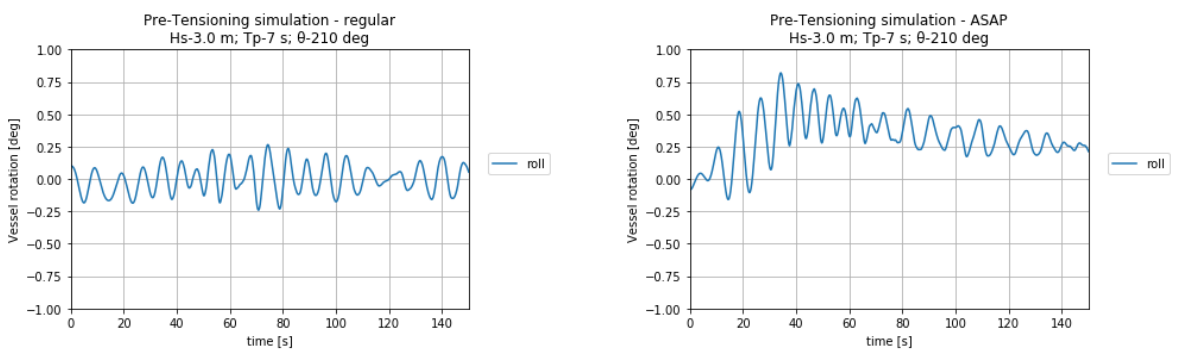


Figure 5-4 Roll motion of the vessel

5.1.1. Evaluation of pre-tensioning schemes

In order to make a fair comparison between the different pre-tensioning schemes and to evaluate the vessel behaviour in different sea states, the following is presented for sea states with a significant wave height of 2.0 meter. The maximum amplitude of the peaks in the dynamic hook load is obtained per simulation. Figure 5-5 shows the average value of these maxima, the maximum value found per sea state is presented in Figure 5-6.

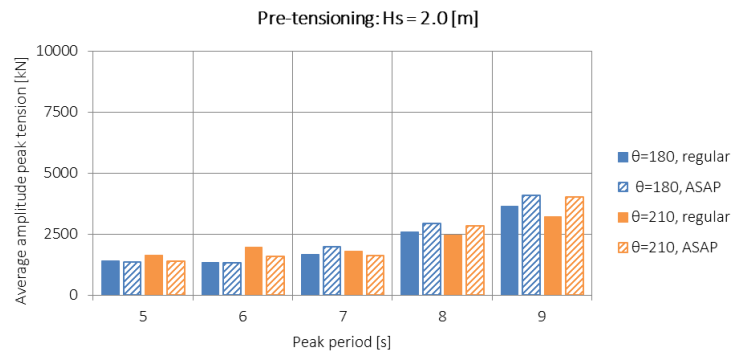


Figure 5-5 Average of the maxima of the amplitude of the dynamic hook load

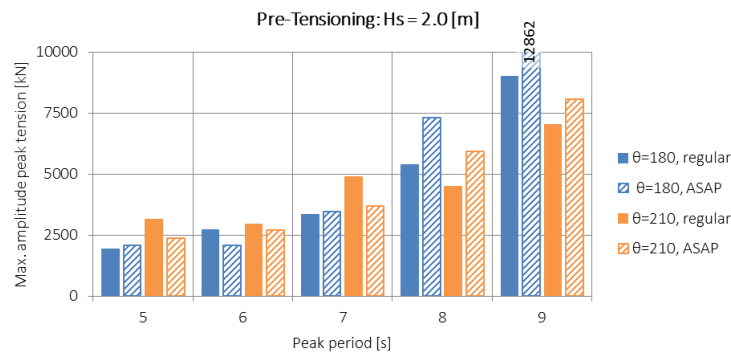


Figure 5-6 Maximum amplitude of the dynamic hook load

In general, the figures show that the highest amplitude of the snap loads occurs for the sea states with a peak period of 8 and 9 seconds, which approach the vessels natural periods of the heave and pitch modes. Therefore, for an increasing peak period the amplitude of the vertical displacement and velocity of the crane tip increase. Due to the coupling of these modes, this is most significant for a wave direction of 180 degrees due to the excitation of the pitch mode for this direction of wave loading. The higher hoisting speed applied in the ASAP pre-tensioning scheme leads to a larger increase the amplitude of the vertical velocity of the hook due to the first snap load. This increases the mean and maximum encountered amplitudes of the dynamic hook load for the peak periods of 8 and 9 seconds.

The scatter of the results for the two highest peak periods considered in the graphs above can be seen in Figure 5-7. Different aspects that influence the height of the maximum value for the simulations of the same sea state are distinguished. The phase of the vertical motion of the hook at which the first snap load occurs is one of the aspects. This determines the increase in vertical velocity due to the first snap load. Next to that, the initial amplitude of the velocity depends on the vessel response to the irregular wave loading, causing the motions of the crane tip. Due to the irregular sea state, the wave height at which the snap loads occur differ for the simulations. As the significant wave height is defined as the mean of the highest $1/3^{\text{rd}}$ of the waves in that particular sea state, this causes part of the variation in the results.

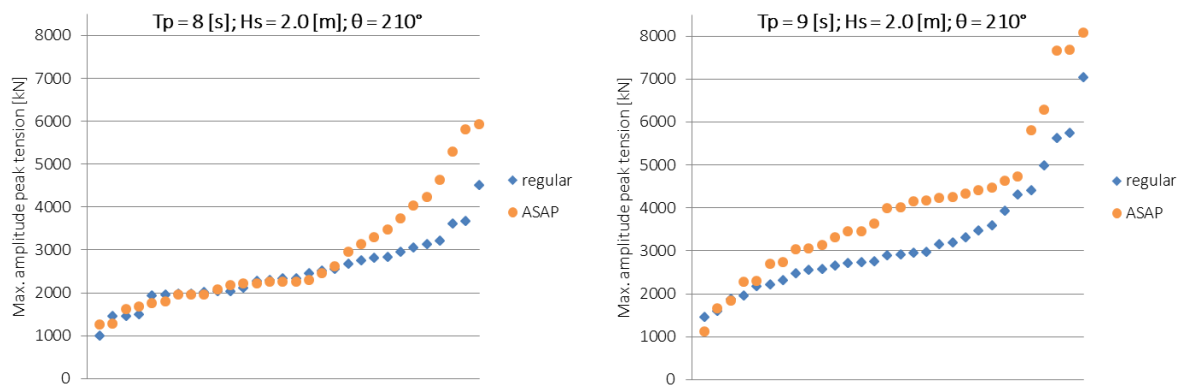


Figure 5-7 Distribution of the maximum peak tension during pre-tensioning

5.2. Lift simulations

When the topside is no longer rigidly connected to the jacket support structure, the lift of the topside is performed. Despite the significant amplitudes of the tension variation for sea states with a peak period lower than 6 seconds, the transition from the constraint to the coupled configuration has shown to be a very fluent one. This is illustrated by the maximum encountered dynamic amplitude factor (DAF) for all simulations for all sea states, which is 1.022 for peak periods up to 5 seconds. The full results can be seen in Appendix C. This section focusses on sea states with a peak period of 7 seconds.

For the graphs shown in this paragraph, simulations that resulted in average values of the loads are used. First the two lifting schemes are evaluated, for which the man-made conical shaped cut is used. Consistently the results of the regular lifting scheme, throughout which the vessel remain in even-keel conditions, are shown on the left. After that, the machine-made carousel shaped cut is evaluated based on the regular lifting scheme. Conclusively, other sea states and the limiting criteria are discussed.

During the first period of the simulations performed, the anti-heeling system increases the counter moment and thereby the average tension in the hoisting system. The dynamic hook load is shown in Figure 5-8. As long as the tension variation does not exceed the static hook load of the topside, the topside remains supported by the jacket legs. The vertical displacement of the topside is shown in Figure 5-9. The impact due to a temporary lift off of the topside results in a drop in the dynamic hook load. As expected, these do hardly occur for the lifting scheme where the maximum hoisting speed is applied before the anti-heeling system has provided the full counter moment corresponding to the heeling moment that the lifted topside exerts at the system. Consequently, the vessel is subject to heel, as can be seen from Figure 5-10. The rapid lift and the heel angle of the vessel result in larger motions and rotations of the topside. Accordingly, larger horizontal displacements of the topside mean larger offlead- or sidelead angles and corresponding horizontal crane loads.

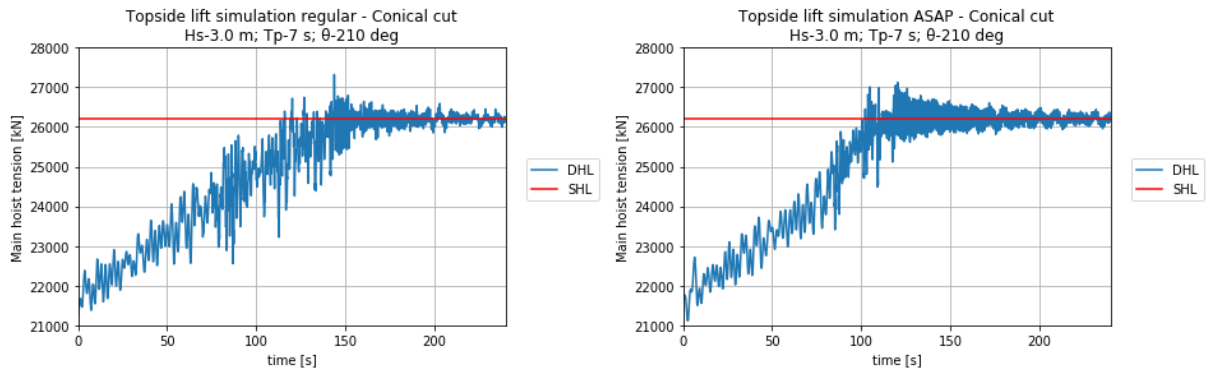


Figure 5-8 Dynamic hook load during lift of the topside

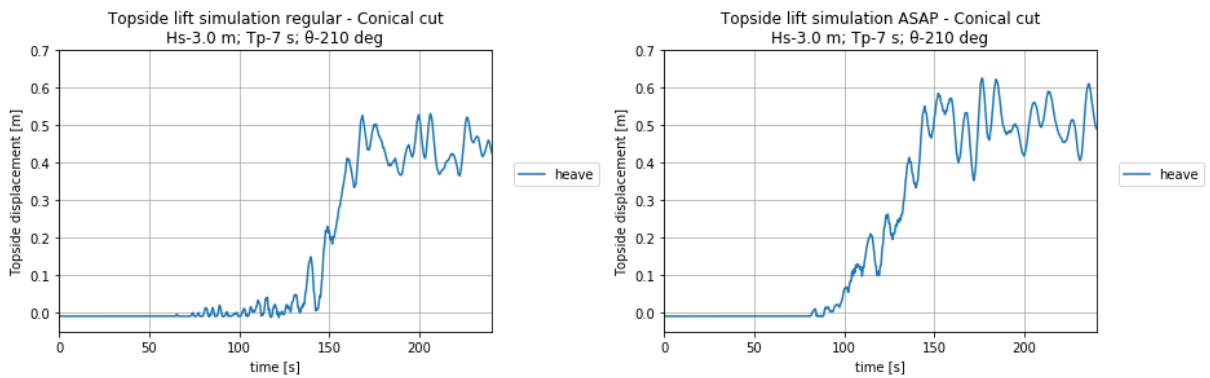


Figure 5-9 Vertical displacement of the topside displacement during the lift operation

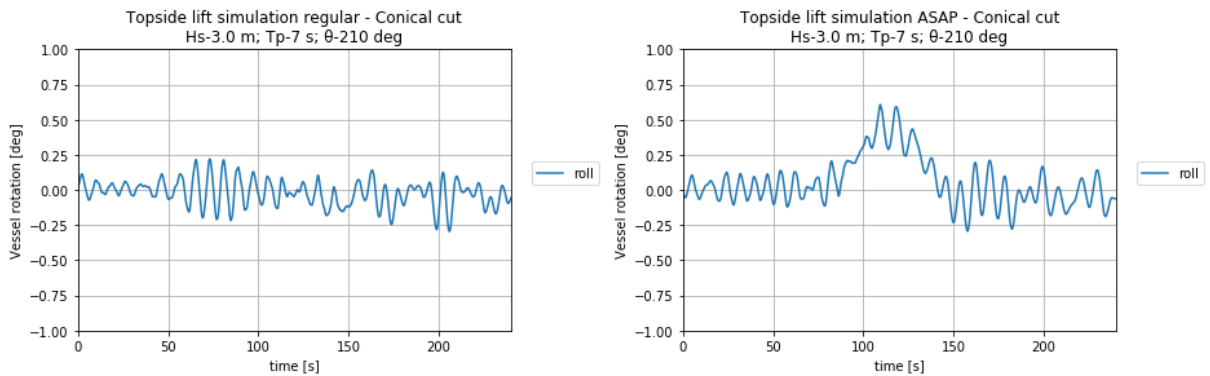


Figure 5-10 Vessel roll angle during the lift operation

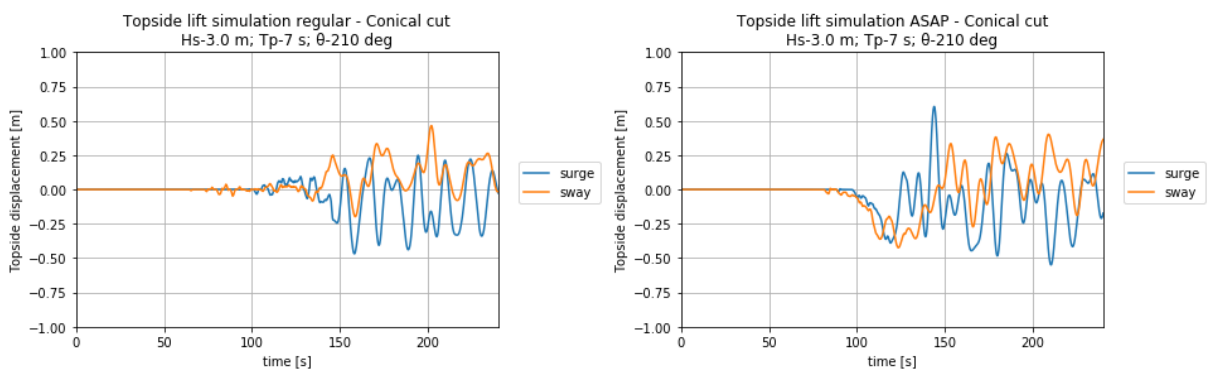


Figure 5-11 Horizontal displacement of the topside during the lift operation

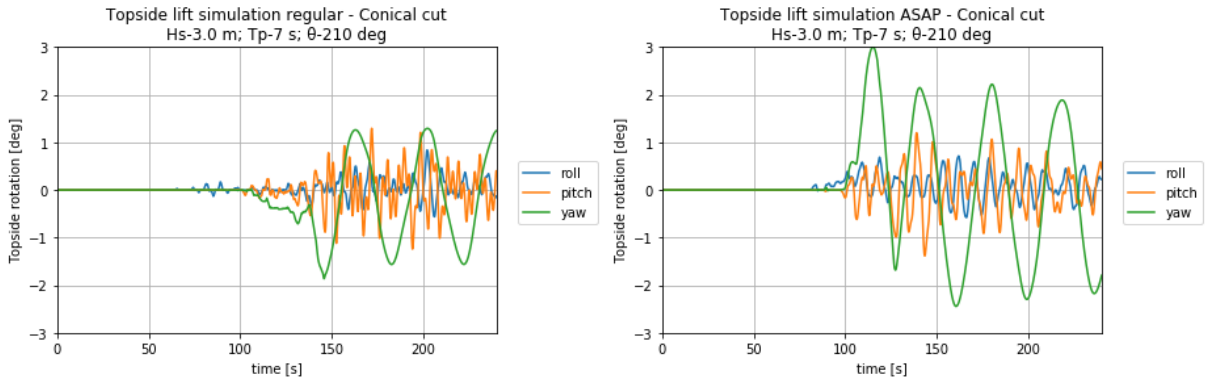


Figure 5-12 Rotations of the topside during the lift operation

The horizontal displacements and yaw motion of the topside are limited by the use of tugger lines that are connected to the crane boom. Next to this, bumpers can be used. Due to the geometry of the carousel cut type, this can be seen as a guided lift for the start of the lift phase. Results for a simulation with this cut can be seen in Figure 5-13. During the transient lift phase, throughout which the impact loads occur, the topside is only able to move in vertical direction. This results in a lower amplitude of the rotations and the sway motion of the topside. Due to friction forces at the vertical surfaces for small topside motions, the vertical displacement of the topside encounter more resistance.

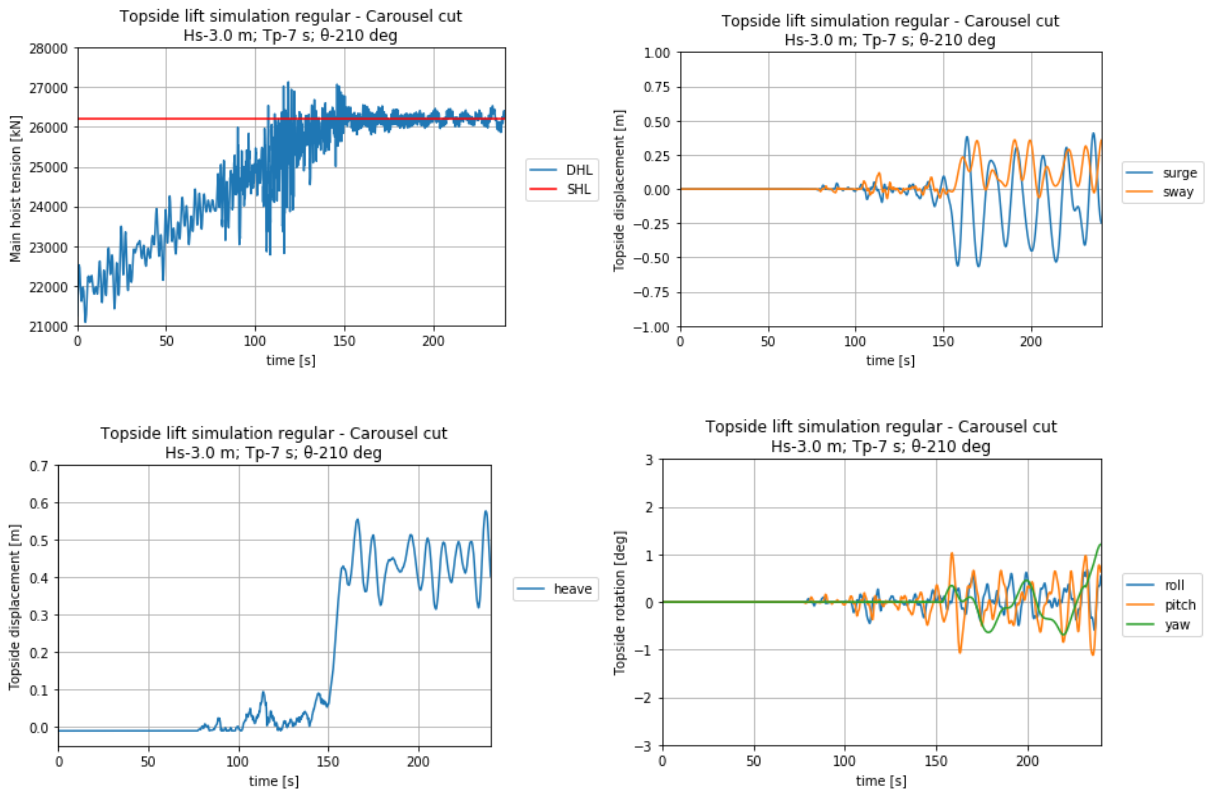


Figure 5-13 Regular lift simulation with the carousel cut

5.2.1. Evaluation of lift schemes and leg cuts

A comparison between the different lifting schemes and the different leg cuts is made for a significant wave height of 2.0 m, the recommended significant wave height for lift operations by the regulations (Det Norske Veritas, 2014a). The maximum values found for the operational criteria (listed in paragraph 2.7) are presented in the tables below. With respect to the regular lift simulations where the conical leg cut is used, both the ASAP lifting scheme and the carousel leg cut have achieved their purpose. The guiding function of the geometry of the carousel cut indeed shows to limit the topside motions and rotations. Consequently a reduction of the offlead and sidelead forces at the crane tip is obtained. However, the maximum dynamic hook load has increased as the value for the DAF is higher. Smaller values for the DAF are found for the ASAP lift scheme, due to the fewer occurring impact loads. However, the topside motions in transverse direction of the vessel (TS sway) are increased due to the heel angle that the vessel is subject to during the lift off of the topside.

Table 5-1 Comparison lift loads and topside motions

$\theta = 180$ [deg] $T_p = 7$ [s] $H_s = 2.0$ [m]	DAF [-]	Offlead [kN]	Sidelead [kN]	Clearance TS-boom [m]	TS surge [m]	TS sway [m]	TS roll [deg]	TS pitch [deg]	TS yaw [deg]
criteria	1.233	1175	1175	3.00	1.50	1.50	2.00	2.00	3.00
ASAP lift Conical cut	1.035	401	447	4.01	0.71	0.84	0.52	1.13	2.95
Regular lift Conical cut	1.040	324	469	4.02	0.94	0.59	0.57	1.56	2.29
Regular lift Carousel cut	1.060	297	406	4.11	0.55	0.37	0.44	0.93	1.52

Table 5-2 Comparison lift loads and topside motions

$\theta = 210$ [deg] $T_p = 7$ [s] $H_s = 2.0$ [m]	DAF [-]	Offlead [kN]	Sidelead [kN]	Clearance TS-boom [m]	TS surge [m]	TS sway [m]	TS roll [deg]	TS pitch [deg]	TS yaw [deg]
criteria	1.233	1175	1175	3.00	1.50	1.50	2.00	2.00	3.00
ASAP lift Conical cut	1.041	498	384	3.70	0.61	1.01	0.77	1.21	2.95
Regular lift Conical cut	1.047	329	424	3.86	0.67	0.55	0.69	1.25	2.61
Regular lift Carousel cut	1.049	287	377	3.91	0.58	0.48	0.65	1.05	1.62

Figure 5-14 shows the values of the dynamic amplitude factor. The spreading in the results is driven by the environmental conditions, as a JONSWAP spectrum is used to compose an irregular sea state. A higher local wave height at the moment of the lift off of the topside can result in higher impact loads due to larger motions of the crane tip. Consequently the dynamic hook load increases.

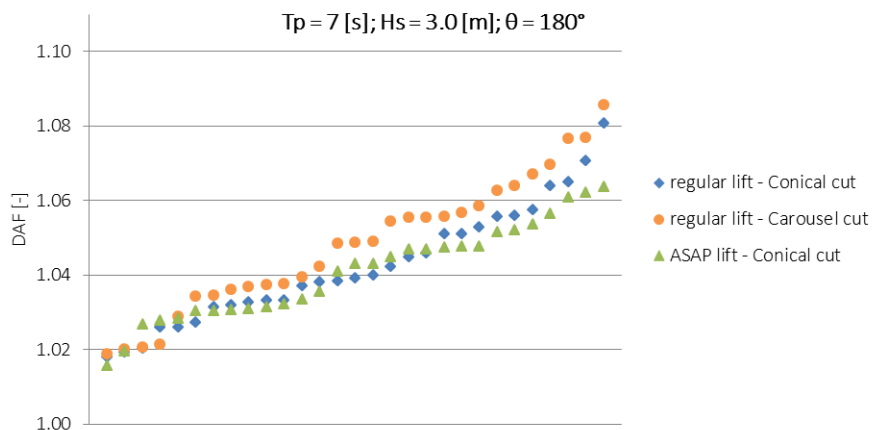


Figure 5-14 Distribution of the dynamic amplitude factor during the lift of the topside

5.2.2. Operational limitations

The sea states used for the evaluation in the previous section show that the BOKALIFT 1 is well capable of performing the single-lift decommissioning operation, as the maxima presented are not close to the limiting criteria, except for the yaw motion of the topside. This rotation of the topside is exceeded for sea states with a higher significant wave height or a higher peak period. Increasing the tension in the tugger lines or controlling their length based on a constant tension could be a solution. Even for a peak period of 8 seconds and a significant wave height of 2.0 meter, the operation can safely be performed if the yaw motions can be controlled in that way.

For a significant wave height higher than 2.0 meter or a peak period longer than 8 seconds, the crane tip motions increase such that the horizontal excursion of the topside can exceed the operational limit of 1.5 meter. Consequently the horizontal crane capacity, the offlead and sidelead loads, can be exceeded. Next to that, the roll and pitch rotations of the topside are exceeded. Bumpers can be installed to keep these motions and loads within the limits, but a trade-off should be made between the additional costs or financial losses due to downtime of the vessel.

Chapter 6. Conclusions and recommendations

During a decommissioning operation, the vessel behaviour is subject to change when the crane hook is attached to the fixed topside and when the topside is lifted. At the transition phases, the transient phenomena of snap loading of the rigging lines and impact loads of the topside at the jacket substructure can occur during the pre-tensioning- and the lift phases, respectively. Since the BOKALIFT 1 is yet to perform its first lift by the time of this study, no operational experience is available. Therefore, the main objective of this thesis reads:

“Evaluate the behaviour of the BOKALIFT 1 during the transient phases of a decommissioning operation”

Time domain simulations are performed for the pre-tensioning and the lift phases, for which the simulation software OrcaFlex is used. First, general conclusions on the vessel behaviour are given. After that, the conclusions and recommendations from the time domain simulations performed on the pre-tensioning phase and the lift phase are presented.

Vessel behaviour

- When the hoisting system is pre-tensioned, the main hoist tackles can be seen as a semi-rigid bar between the hook and the crane tip, which is hinged at both ends. This constrains the motions of the crane tip and shifts the centre of rotation of the vessel to the hook. Due to the location and orientation of the crane, the mode shapes and the corresponding natural periods of the vessel motions are subject to change.
- When the motions of the crane tip are constrained, the stiffness of the hoisting system significantly reduces the natural period of the roll mode of the vessel. Next to this, the roll mode is coupled with the heave degree of freedom due to the shift of the centre of rotation.
- The stiffness of the hoisting system does not affect the natural periods of the heave and pitch modes of the vessel when the motions of the crane tip are constrained. However, the constrain does affect the shape of these modes. A roll component is present in the heave mode and, to a lesser extent, the pitch mode of the vessel. This coupling has shown to be dictating the roll motion of the vessel.

An OrcaFlex model representing the constrained conditions is used to perform time domain simulations to define the workability of the vessel. Hereby the highest allowable significant wave height per peak period is obtained. Wave direction of 180 and 210 degree are investigated. The horizontal components of the crane loads, the offlead and sidelead forces, are the limiting criteria. With these simulations, the maximum amplitude of the tension variation of the dynamic hook load due to the wave induced vessel motions is determined. Thereby, the first sub-objective is achieved.

Pre-tensioning phase

Two pre-tensioning schemes are evaluated, which differ in hoisting speed and the moment when the anti-heeling system starts to correct the heeling moment. The conclusions on the pre-tensioning simulations are presented below.

- The results of all simulations, performed for all sea states investigated, remained within the strength requirements and operational limitations. This confirms the validity of the defined workability limits for the pre-tensioning phase.
- Only for sea states with a peak period of 5 seconds or higher, the amplitude of the dynamic hook load due to the snap loads in the rigging lines can be significantly larger than the maximum amplitude of the tension variation due to the wave induced vessel motions.

- The largest peaks of the dynamic hook load due to the snap loading of the rigging lines occurs for sea states with a peak period of 8 and 9 seconds, which is near the natural period of the heave and pitch modes of the vessel. Therefore, the largest amplitude of the vertical motions and velocities of the crane tip and crane hook are encountered in these sea states. Due to the coupling of these modes, the highest snap loads are found for a wave direction of 180 degrees.
- For this configuration, pre-tensioning cannot fully be performed by reducing the tackle length only due to the weight of the rigging lines. The counter moment applied by the anti-heeling system is needed to obtain the tension in the hoisting system for which the rigging lines are taut.
- For the simulations where the maximum hoist speed is applied, the snap loads cause a larger increase of the amplitude of the vertical velocity of the crane hook. Consequently, larger snap loads occur. Therefore, it is not recommended to use the maximum hoisting speed for the pre-tensioning in sea states with a peak period of 7 second or higher. For the pre-tensioning phase, this answers the sub-objective to investigate the influence of the hoisting speed on the crane loads.

Lift phase

Two lifting schemes are evaluated for the time domain simulations of the lift of the topside. Next to that, two geometries for the cut of the jacket leg are assessed. The conclusions on the simulations of the lift phase are presented below.

- The BOKALIFT 1 has shown to be well-suited for a decommissioning operation. Up to a sea state with a peak period of 7 seconds and the recommended maximum significant wave height of 2.0 meter, no operational criteria are exceeded. If the pitch and yaw motions of the topside can be controlled by changes to the tugger lines, the operation can also be safely performed for sea states with a significant wave height of 2.0 meter and a peak period of 8 seconds.
- For higher peak periods or a higher significant wave height, the motions of the topside can exceed the operational limits. Hereby the horizontal crane loads are exceeded too. The workability of the vessel can be increased up to sea states with a peak period up to 9 seconds when bumpers are used to limit the horizontal topside motions. Hereby the third sub-objective is achieved.
- The lift scheme in which the hoisting speed is increased before the full counter moment is provided by the anti-heeling system results in a lower dynamic amplitude factor. However, the horizontal crane loads increase due to larger motions of the topside. The motions in transverse direction of the vessel are a consequence of the heel angle of the vessel during the lift phase. For the lift phase, this answers the second sub-objective.
- Smaller motions and rotations of the topside are obtained from the simulations where the machine-made carousel cut type is used. Its geometry has shown to have a guiding function during the lift operation. Due to friction at the vertical contact area during the impact loads the dynamic amplitude factor increases. This is the conclusion on the last sub-objective.
- According to the maximum encountered dynamic amplitude factor of 1.06 for the lift simulations performed for a sea state with a peak period of 7 seconds and the recommended significant wave height of 2.0 meters, the lift of topsides with a larger weight than 2,500 tonne can be investigated.

Conclusively, it is recommended to limit the impact loads by an increase of the hoist speed before the full anti-heeling moment is provided by the anti-heeling system. However, to limit the horizontal topside motions due to the heel angle that the vessel is subject to under these conditions, the tension level for which the lift is started should be reconsidered. Next to that, it is recommended to use the machine-made carousel cut of the jacket legs when this is possible. The geometry limits the topside motions and rotations by which the topside is easier to handle during the lift.

- Balmoral Marine. (2004). *Marine Equipment Handbook*.
- Boskalis. (2016a). Equipment Sheet - Overview. Retrieved September 12, 2016, from <http://boskalis.com/download-center.html>
- Boskalis. (2016b). *OE16DP011-CN-002 Roll Damping calculation note*.
- Boskalis. (2017). Equipment Sheet - Bokalift 1. Retrieved April 24, 2017, from <https://boskalis.com/about-us/fleet-and-equipment/offshore-vessels/heavy-lift-vessels.html>
- Danish Meteorological Institute. (2016). North Sea - Baltic Sea ocean model. Retrieved February 16, 2017, from <http://ocean.dmi.dk/models/hbm.uk.php>
- Decom North Sea. (2014). *Review of Decommissioning Capacity*.
- Decom North Sea. (2015). *Offshore Oil and Gas Decommissioning*.
- Det Norske Veritas. (2007). DNV-RP-C205 Environmental conditions and environmental loads.
- Det Norske Veritas. (2014a). DNV-OS-H205 Lifting Operations (VMO Standard - Part 2-5).
- Det Norske Veritas. (2014b). DNV-RP-H201 Lifting appliances used in subsea operations.
- Det Norske Veritas. (2016). DNVGL-ST-N001 Marine operations and marine warranty.
- Gourvenec, S., & Techera, E. (2016). Rigs to reefs: is it better to leave disused oil platforms where they stand? Retrieved September 25, 2016, from <http://theconversation.com/rigs-to-reefs-is-it-better-to-leave-disused-oil-platforms-where-they-stand-63670>
- Heavy Lift PFI. (2016). Huisman wins heavy lift orders. Retrieved September 15, 2016, from <http://www.heavyliftpfi.com/news/huisman-wins-heavy-lift-orders.html>
- Huisman Equipment B.V. (2015). Huisman Cranes. Retrieved September 16, 2016, from <http://www.huismanequipment.com/en/products/cranes>
- International Maritime Organisation. (1989). 1989 Guidelines and Standards for the Removal of Offshore Installations and Structures on the Continental Shelf and in the Exclusive Economic Zone, (IMO Resolution A.672 (16)).
- International Maritime Organisation. (1994). Guidelines for Vessels with Dynamic Positioning Systems, (IMO MSC.Circ.645).
- Irvine, H. (1981). *Cable Structures*. Cambridge: The MIT Press.
- Journée, J. M. J., & Massie, W. W. (2001). *Offshore Hydromechanics*. Delft University of Technology.
- Jumbo Maritime. (2016). Jumbo fleet. Retrieved September 14, 2016, from <https://www.jumbomaritime.nl/en/shipping/>
- Macreadie, P. I., Fowler, A. M., & Booth, D. J. (2011). Rigs-to-reefs: Will the deep sea benefit from artificial habitat? *Frontiers in Ecology and the Environment*, 9(8), 455–461. <http://doi.org/10.1890/100112>
- MARIN. (2016). Safetrans 7.0 Theory Manual.

Martin, A. T. (2003). Decommissioning of International Petroleum Facilities evolving Standards & Key Issues. *Oil, Gas & Energy Law*, (5). Retrieved from <http://www.ogel.org/article.asp?key=765>

OSPAR Commission. (1998). *Ministerial Meeting of the OSPAR Commission*. Sintra.

Palantir. (2014). Decommissioning in the UKCS. Retrieved September 30, 2016, from <http://www.palantirsolutions.com/decommissioning-and-the-ukcs/>

Seaway Heavy Lifting Engineering B.V. (2016). Vessels - Technical specifications. Retrieved September 14, 2016, from <https://www.seawayheavylifting.com.cy/vessels>

UNCLOS. 1958 Convention on the Continental Shelf (1958). United Nations. Retrieved from http://treaties.un.org/doc/Treaties/1964/06/19640610 02-10 AM/Ch_XXI_01_2_3_4_5p.pdf

List of figures

Figure 1-1 F-class Semi-Submersible Heavy Transport Vessel Finesse	1
Figure 1-2 Artist impression Heavy Lift Vessel BOKALIFT 1	1
Figure 1-3 World's largest crane vessel – Sleipnir (Heerema Marine Contractors).....	2
Figure 1-4 Huisman Offshore Mast Crane (Huisman Equipment B.V., 2015)	2
Figure 1-5 Crane nomenclature	2
Figure 1-6 Alternative decommissioning options (Macreadie et al., 2011)	3
Figure 1-7 Fields to be decommissioned in the near future (Palantir, 2014)	4
Figure 1-8 Boskalis' floating sheerleg vessels Taklift 4 and Taklift 7	5
Figure 1-9 Qualitative representation of the tension in the hoisting wires over decommissioning process	8
Figure 1-10 Qualitative representation of the impact load phenomenon	9
Figure 2-1 OrcaFlex model	13
Figure 2-2 General arrangement decommissioning operation	14
Figure 2-3 General arrangement BOKALIFT 1 and mast crane	14
Figure 2-4 Crane nomenclature	17
Figure 2-5 Mast crane model	17
Figure 2-6 Offlead angle (left) and Sidelead angle (right)	18
Figure 2-7 Redistribution of ballast water load in designated anti-heeling water ballast tanks	19
Figure 2-8 Start and end location of the anti-heeling mass	19
Figure 2-9 Top view model of horizontal vessel constraints	20
Figure 2-10 Topside model	21
Figure 2-11 Models of the Conical cut (left) and Carousel cut (right)	21
Figure 2-12 Leg cut detail	22
Figure 3-1 Modal analysis: model of the uncoupled configuration	23
Figure 3-2 Modal analysis: model of the coupled configuration	24
Figure 3-3 Modal analysis: model of the coupled configuration – top view	24
Figure 3-4 Modal analysis: model of the constraint configuration	25
Figure 3-5 Vessel heave mode – constraint model.....	26
Figure 3-6 Undamped natural periods of the anti-symmetric vessel modes	27
Figure 3-7 Undamped natural periods of the symmetric vessel modes.....	27
Figure 4-1 Water depth North Sea (Danish Meteorological Institute, 2016).....	29
Figure 4-2 Wave directions	29
Figure 4-3 Tackle length versus anti-heeling mass location for even-keel conditions	30
Figure 4-4 Main hoist tension versus tackle length for even-keel conditions.....	31
Figure 4-5 Pre-tensioning schemes	33
Figure 4-6 Hoisting schemes for the lift phase	34
Figure 5-1 Main hoist tension	36
Figure 5-2 Vertical motions of the crane tip and crane hook	36
Figure 5-3 Vertical velocity of the crane tip and crane hook	36
Figure 5-4 Roll motion of the vessel	36
Figure 5-5 Average of the maxima of the amplitude of the dynamic hook load	37
Figure 5-6 Maximum amplitude of the dynamic hook load	37
Figure 5-7 Distribution of the maximum peak tension during pre-tensioning	38
Figure 5-8 Dynamic hook load during lift of the topside	39
Figure 5-9 Vertical displacement of the topside displacement during the lift operation	39
Figure 5-10 Vessel roll angle during the lift operation	39
Figure 5-11 Horizontal displacement of the topside during the lift operation	39
Figure 5-12 Rotations of the topside during the lift operation	40

Figure 5-13 Regular lift simulation with the carousel cut	40
Figure 5-14 Distribution of the dynamic amplitude factor during the lift of the topside	41
Figure C-1 Modal analysis: model of the coupled configuration	57
Figure C-2 Modal analysis: model of the coupled configuration – top view	57
Figure C-3 Vessel surge mode – constraint model	59
Figure C-4 Vessel sway mode – constraint model	59
Figure C-5 Vessel heave mode – constraint model	59
Figure C-6 Vessel roll mode – constraint model	60
Figure C-7 Vessel pitch mode – constraint model	60
Figure C-8 Vessel yaw mode – constraint model.....	60

List of tables

Table 2-1 General arrangement decommissioning operation	13
Table 2-2 Particulars BOKALIFT 1.....	13
Table 2-3 Characteristics movement anti-heeling mass	20
Table 3-1 Degrees of freedom per rigid body per configuration.....	23
Table 3-2 Mode shape coefficients of the uncoupled configuration	24
Table 3-3 Mode shape coefficients of the coupled configuration	25
Table 3-4 Vessel mode shape coefficients of the constraint configuration	26
Table 3-5 Natural periods symmetric vessel motions including added mass	28
Table 4-1 Sea states.....	30
Table 4-2 Maximum significant wave height (H_s in [m]) per peak period	31
Table 4-3 Maximum amplitude of the tension variation [kN] - Lift phase	32
Table 4-4 Maximum amplitude of the tension variation [kN] – Pre-tensioning phase	32
Table 5-1 Comparison lift loads and topside motions.....	41
Table 5-2 Comparison lift loads and topside motions.....	41
Table C-1 Modal analysis coupling coefficients – Uncoupled system	58
Table C-2 Modal analysis coupling coefficients – Constraint system, anti-heeling mass at the centre line	58
Table C-3 Modal analysis coupling coefficients – Constraint system, anti-heeling mass at its final location	58
Table C-4 Modal analysis coupling coefficients – Coupled system.....	58
Table C-5 Mean of the maximum amplitudes snap loads [kN] per sea state	61
Table C-6 Maximum amplitude snap loads [kN] per sea state	61
Table C-7 Maximum amplitude of the tension variation	62
Table C-8 Maximum amplitude of the tension variation	62
Table C-9 Evaluation operational criteria – regular lift scheme - conical cut	63
Table C-10 Evaluation operational criteria – regular lift scheme - conical cut	63
Table C-11 Maximum crane loads – ASAP lift scheme - conical cut	63
Table C-12 Maximum crane loads – ASAP lift scheme - conical cut	63
Table C-13 Maximum crane loads – regular lift scheme - carousel cut	64
Table C-14 Maximum crane loads – regular lift scheme - carousel cut	64

OrcaFlex is simulation software that is widely used in the offshore engineering business to analyse the dynamics of offshore marine systems. Its applications range from designing mooring systems to pipelay dynamics. Certain aspects of the software and the use of it is given in this appendix.

A.1. Components

The graphical user interface in OrcaFlex allows the user to use several objects, that can be seen as building blocks, with different properties that can be linked to each other by several components. It is therefore very user friendly and on this manner dynamic multi-body systems in a marine environment can be modelled. The objects and linking components available are discussed below.

Vessel

An object with all 6 degrees of freedom (translation along- and rotation around X, Y and Z axis) that responds to wave loads, applied loads and forces due to interaction with other components linked to it. For this object and the 6D Buoy and lines, it is possible to select whether or not to include certain types of environmental loading. The vessel behaviour is simulated based on displacement- and/or load RAO, the hydrodynamic stiffness matrix and the frequency dependent added mass- and damping matrices, which can be obtained from a diffraction analysis.

Line

An object that can be used to model catenary- or taut mooring lines, pipelines, cables, risers and other slender objects. A line type can be given mass per unit length, diameter (to determine its volume – subject to drag), stiffness (axial, bending and torque) and (material- or Rayleigh-) damping characteristics and can account for buoyancy, added mass, drag, torsion and (axial-) extension. The line properties are discretised using a model of lumped masses interconnected by a spring and a dashpot. The lumped masses have 6 degrees of freedom each.

3D Buoy

A 3D Buoy object is a point mass that has the translational degrees of freedom only. Characteristics that can be given to a 3D Buoy object are mass, volume and drag area. Their motions account for buoyancy, drag, added mass and interaction with shapes. Only lines or other linking objects can be connected to it.

6D Buoy

An object with 6 degrees of freedom (translation along- and rotation around X, Y and Z axis). In addition to the characteristics for a 3D Buoy, mass moments of inertia are required for the rotational degrees of freedom and can therefore account for moments applied to it. Next to that it can account for slamming, supports can be added, forces can be applied to it and it can be given a geometry. The geometry consists of edges. Contact with shapes can be modelled and forces are applied when multiple edges form a contact area with the shape.

Shape

An object that has normal- and shear stiffness properties and acts as an obstacle. It should be fixed at a relative location with respect to a reference system, being the global reference system or the local axis system of a vessel, 3D-buoy, 6D-buoy or a line node. It allows to model contact with buoys and lines. Damping is only available if the explicit integration scheme is used.

Winch

A massless component that can connect two objects by a wire which is given a certain axial stiffness. The winch can control the wire length or the tension in the wire over a time domain simulation according to values of

length, (wire-) pay-out or tension predefined for certain moments in time. It only accounts for elongation of the wire.

Link

A massless spring component that can connect to two objects or one object with the global reference system. It is implemented as a tether (a spring that cannot be compressed) or as a spring-dashpot.

Constraint

A component that can be used to limit the degrees of freedom of vessel-, 6D buoy-, 3D buoy-objects and line nodes. It has no other characteristics than a location of implementation relative to the linked object. Introduced recently in OrcaFlex release 10.1a.

Appendix B. Diffraction analysis

The objective of the simulations described in this chapter is to obtain and to compare the Response Amplitude Operators (RAO) of the vessel (BOKALIFT 1) for different hook loads in the scope of a decommissioning operation. The RAO are transfer functions between the wave amplitude and the amplitude of forces on the vessel / motions of the vessel per frequency (respectively called load RAO and displacement RAO). Since load RAO (are assumed to) only depend on the geometry of the vessel (see equations (B.21) and (B.22)) these are expected to remain constant for the different simulations, whereas the displacement RAO, solved from the equation of motion, are expected to change due to differences in mass properties.

B.1. ANSYS AQWA

AQWA is used to perform diffraction calculations from which load- and displacement RAO are obtained. These are calculated with respect to the Centre of Gravity (CoG) of the body. As a part of finite element calculation software package ANSYS 16.1, the AQWA Suite contains calculation tools regarding hydrodynamics which can perform several static or dynamic simulations on one (or multiple) floating body/bodies. The calculations can be performed in the frequency domain or in the time domain. A mesh is created to describe the actual shape of the body and is made up from triangular- and quadrilateral pressure plate elements, defined by 3 or 4 nodes, respectively. The nodes are defined with respect to a global, fixed, right handed axis system OXYZ with the origin in the mean free surface of the fluid and the z-axis pointing vertically upwards. For each body a local, right handed axis system Gxyz is defined fixed to its CoG.

Product information can be found at: <http://www.ansys.com/products/structures/ansys-aqwa>

B.2. Potential theory and diffraction analysis

A floating body, considered rigid with no forward speed, in a homogeneous fluid and in a continuous domain, can be described by a mass-spring-dashpot system with 6 degrees of freedom (3 translational, 3 rotational). The equation of motion of the body in its CoG (in matrix notation) reads as follows:

$$(\mathbf{M} + \mathbf{A})\ddot{\underline{x}}(t) + \mathbf{C}\dot{\underline{x}}(t) + \mathbf{K}\underline{x}(t) = \underline{F}(t) \quad (\text{B.1})$$

Where:	\underline{x}	displacement vector (with respect to its equilibrium position)
	\mathbf{M}	Mass matrix
	\mathbf{A}	Added mass matrix
	\mathbf{C}	Damping matrix
	\mathbf{K}	Stiffness matrix
	\underline{F}	Hydrodynamic loads on the floating body

The mass and stiffness matrix are properties of the floating body itself. From (hydro-)statics, considering only the stiffness and forces that do not vary over time (gravity), the initial conditions (displacements and rotations) can be determined. The added mass and damping coefficients and the hydrodynamic wave loads are to be determined from the interaction with the environment. In this paragraph, the notation used in (Journée & Massie, 2001) is followed.

Motions are driven by energy. The energy in the system can be split up into kinetic and potential energy of the body and external forces (work done = force * time). Describing the flow field in the fluid can be done using [mass](#) and [momentum balances](#). The balances can be seen as conservation of mass or momentum over a period Δt in volume $\Delta x \Delta y \Delta z$, which is equal to the sum of the net import + the local production of mass or momentum during that period.

Considering the *mass balance*, local production of mass is not possible. With the assumption that the fluid is [incompressible](#) this leads to the [continuity condition](#):

$$\frac{\partial \rho}{\partial t} + \frac{\partial \rho u_x}{\partial x} + \frac{\partial \rho u_y}{\partial y} + \frac{\partial \rho u_z}{\partial z} = S_\rho \xrightarrow{\text{incompressible}} \frac{\partial u_x}{\partial x} + \frac{\partial u_y}{\partial y} + \frac{\partial u_z}{\partial z} = 0 \quad (\text{B.2})$$

The fluid flow can be described by a potential function regarding the velocity potential. Along a certain potential line, the value of the potential remains constant. With the velocity $u(t)$ in each (x, y and z) direction, the [velocity potential function](#) is defined as follows:

$$\Phi(x, y, z, t) \quad \text{such that} \quad u_x = \frac{\partial \Phi}{\partial x} \quad u_y = \frac{\partial \Phi}{\partial y} \quad \text{and} \quad u_z = \frac{\partial \Phi}{\partial z} \quad (\text{B.3})$$

Rewriting the continuity condition with the definition of the velocity potential leads to the [Laplace equation](#) (where ∇ denotes spatial derivatives):

$$\nabla^2 \Phi = \frac{\partial^2 \Phi}{\partial x^2} + \frac{\partial^2 \Phi}{\partial y^2} + \frac{\partial^2 \Phi}{\partial z^2} = 0 \quad (\text{B.4})$$

Considering the *momentum balance*, conservation of momentum is only valid for [inviscid](#) fluids, meaning that no energy can be lost due to the presence of vortices, friction or shear forces in the fluid. The production of momentum that remains is the sum of forces on volume $\Delta x \Delta y \Delta z$ induced by pressure and gravity only. Momentum (and the change of momentum over time) should be considered per direction. The (therefore 3) momentum balance equations become:

$$\frac{\partial(\rho u_i)}{\partial t} + \frac{\partial u_x(\rho u_i)}{\partial x} + \frac{\partial u_y(\rho u_i)}{\partial y} + \frac{\partial u_z(\rho u_i)}{\partial z} = S_i \quad \text{for } i = x, y, z \quad (\text{B.5})$$

where S_i is the local production of momentum:

$$S_x = -\frac{\partial p}{\partial x} \quad S_y = -\frac{\partial p}{\partial y} \quad S_z = -\frac{\partial p}{\partial z} - \rho g \quad (\text{B.6})$$

Applying the *continuity equation* to the momentum balances leads to the [Euler equations](#):

$$\begin{aligned} \frac{\partial u_x}{\partial t} + u_x \frac{\partial u_x}{\partial x} + u_y \frac{\partial u_x}{\partial y} + u_z \frac{\partial u_x}{\partial z} &= -\frac{1}{\rho} \frac{\partial p}{\partial x} \\ \frac{\partial u_y}{\partial t} + u_x \frac{\partial u_y}{\partial x} + u_y \frac{\partial u_y}{\partial y} + u_z \frac{\partial u_y}{\partial z} &= -\frac{1}{\rho} \frac{\partial p}{\partial y} \\ \frac{\partial u_z}{\partial t} + u_x \frac{\partial u_z}{\partial x} + u_y \frac{\partial u_z}{\partial y} + u_z \frac{\partial u_z}{\partial z} &= -\frac{1}{\rho} \frac{\partial p}{\partial z} - g \end{aligned} \quad (\text{B.7})$$

Combining the *Euler equations* with the assumption of an [irrotational](#) flow (in the equations regarding the x- and y-direction gz may be added without changing the meaning of the equation):

$$\begin{aligned}\frac{\partial u_x}{\partial t} + \frac{1}{2} \frac{\partial}{\partial x} (u_x^2 + u_y^2 + u_z^2) &= -\frac{\partial}{\partial x} \left(\frac{p}{\rho} + gz \right) \\ \frac{\partial u_y}{\partial t} + \frac{1}{2} \frac{\partial}{\partial y} (u_x^2 + u_y^2 + u_z^2) &= -\frac{\partial}{\partial y} \left(\frac{p}{\rho} + gz \right) \\ \frac{\partial u_z}{\partial t} + \frac{1}{2} \frac{\partial}{\partial z} (u_x^2 + u_y^2 + u_z^2) &= -\frac{\partial}{\partial z} \left(\frac{p}{\rho} + gz \right)\end{aligned}\tag{B.8}$$

Applying the definition of the *velocity potential* leads to the Bernoulli equation:

$$\begin{aligned}\frac{\partial}{\partial x} \left(\frac{\partial \Phi}{\partial t} + \frac{1}{2} |\nabla \Phi|^2 + \frac{p}{\rho} + gz \right) &= 0 \\ \frac{\partial}{\partial y} \left(\frac{\partial \Phi}{\partial t} + \frac{1}{2} |\nabla \Phi|^2 + \frac{p}{\rho} + gz \right) &= 0 \\ \frac{\partial}{\partial z} \left(\frac{\partial \Phi}{\partial t} + \frac{1}{2} |\nabla \Phi|^2 + \frac{p}{\rho} + gz \right) &= 0\end{aligned}\tag{B.9}$$

[Bernoulli Equation:](#)

$$\frac{\partial \Phi}{\partial t} + \frac{1}{2} |\nabla \Phi|^2 + \frac{p}{\rho} + gz = 0\tag{B.10}$$

Summing up the assumptions made to obtain the *Bernoulli equation* expressed with the velocity potential, the fluid is said to be incompressible, irrotational and inviscid. *Note that vortices or shear forces are not possible in irrotational flow anyway and the assumption of an inviscid flow is basically included in the definition of the velocity potential.*

In order to solve the velocity potential function for a flow field, boundary conditions are needed. To use potential flow theory, the following must hold:

- Pressure at the water surface is equal to the atmospheric pressure ([dynamic boundary condition](#))

$$p = 0 \quad \text{at} \quad z = \zeta(x, y, t)\tag{B.11}$$

- No water particles may leave the free water surface ([kinematic boundary condition](#))

$$\frac{\partial \Phi}{\partial z} = \frac{\partial \zeta}{\partial t} \quad \text{at} \quad z = \zeta(x, y, t)\tag{B.12}$$

Assuming the fluid to be incompressible, inviscid and irrotational, and assuming that the amplitude of the motions and velocities are small, the fluid domain (Bernoulli equation and boundary conditions) can be described taking only the linear terms into account.

[Linearised Bernoulli equation:](#)

$$p = -\rho \frac{\partial \Phi}{\partial t} - \rho g z\tag{B.13}$$

Dynamic boundary condition applied at linearised Bernoulli equation at the free surface elevation (ζ):

$$\frac{\partial \Phi}{\partial t} + g\zeta = 0 \quad \text{or} \quad \frac{\partial^2 \Phi}{\partial t^2} + g \frac{\partial \zeta}{\partial t} = 0 \quad \text{at} \quad z = \zeta(t)\tag{B.14}$$

The amplitudes of motions and velocities are assumed to be small. Therefore, combining equations (B.12) and (B.14) and linearising $z = \zeta(t)$ by $z = 0$ leads to the free surface condition:

$$\frac{\partial^2 \Phi}{\partial t^2} + g \frac{\partial \Phi}{\partial z} = 0 \quad \text{at } z = 0 \quad (\text{B.15})$$

Assuming the seabed to be impermeable and flat (combining the free surface condition and the Laplace equation):

$$\frac{\partial \Phi}{\partial z} = 0 \quad \text{at } z = -d \quad (\text{B.16})$$

Considering a fixed body in the flow field adds a (kinematic) boundary condition due to the presence of the obstacle. Taking the surface of the fixed body as impermeable, defining a direction n normal to a surface, positive into the fluid results in:

$$\frac{\partial \Phi}{\partial n} = 0 \quad \text{at the body surface} \quad (\text{B.17})$$

The body's total velocity potential is a superposition of the potentials of the undisturbed incoming wave, the diffracted wave due to the fixed body and the (radiation) potential due to the body oscillating in all its degrees of freedom separately:

$$\Phi = \sum_{j=1}^6 \Phi_{r,j} + \Phi_w + \Phi_d \quad (\text{B.18})$$

Where: Φ_w = undisturbed incoming wave potential ($j = 0$)
 $\Phi_{r,j}$ = radiation potential due to body motions in all degrees of freedom (for $j = 1..6$)
 Φ_d = diffracted undisturbed incoming wave potential ($j = 7$)

The linear response of a floating body with zero forward speed in regular, harmonic waves can be calculated in the frequency domain. Using linear wave theory (or Airy wave theory) a separation of variables regarding time and space can be made. Therefore, all body motions will be described by harmonics. This separates the amplitude of the potential and the harmonic variation in time:

$$\Phi(x, y, z, t) = \phi(x, y, z) \cdot e^{-i\omega t} \quad \text{with} \quad \phi(x, y, z) = -i\omega \sum_{j=0}^7 \phi_j \zeta_j \quad (\text{B.19})$$

The fluid pressure at the floating body now follows from the [linearised Bernoulli equation](#):

$$p(x, y, z, t) = -\rho \frac{\partial \Phi}{\partial t} = \rho \omega^2 \left\{ (\phi_0 + \phi_7) \zeta_0 + \sum_{j=1}^6 \phi_j \zeta_j \right\} \cdot e^{-i\omega t} \quad (\text{B.20})$$

Knowing the pressure distribution along the hull, integrating over the wetted surface area of the hull (S_0) results in the forces. The (first order) forces ($k = 1, 2, 3$) and moments ($k = 4, 5, 6$) in direction k , accounting for the undisturbed incoming wave and diffracted wave are:

$$X_k = -\iint_{S_0} p n_k \cdot dS_0 = -\rho \omega^2 \zeta_0 e^{-i\omega t} \iint_{S_0} (\phi_0 + \phi) n_k \cdot dS_0 \quad (\text{B.21})$$

and the forces and moments accounting for the oscillating motion of the body are:

$$F_k = -\iint_{S_0} p n_k \cdot dS_0 = -\rho \omega^2 \sum_{j=1}^6 \zeta_j e^{-i\omega t} \iint_{S_0} \phi_j n_k \cdot dS_0 \quad (\text{B.22})$$

From the radiation forces found in (B.22), the in-phase (real) part defines the added mass (coupling) coefficients and the out of phase (imaginary) part defines the wave damping (coupling) coefficients. Solving the potentials is done using the Green's function (or influence function).

C.1. Modal Analysis

The OrcaFlex model used for modal analysis of the coupled configuration is presented in the figure below. The normalised coupling coefficients for all configurations can be found in tables afterwards.

Configuration / Model	Difference with previous
Uncoupled	-
Constraint (start)	Introduction fixed topside + rigging lines, connected to the main hoist block
Constraint (end)	Shifted anti-heeling mass from centre line towards its end location (where it applies the maximum counter moment)
Coupled	Topside is no longer fixed, but free

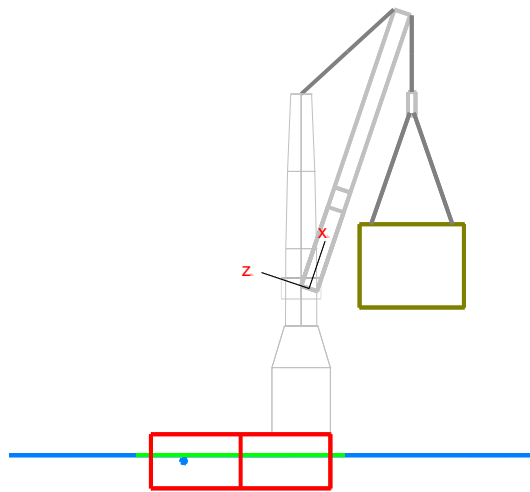


Figure C-1 Modal analysis: model of the coupled configuration

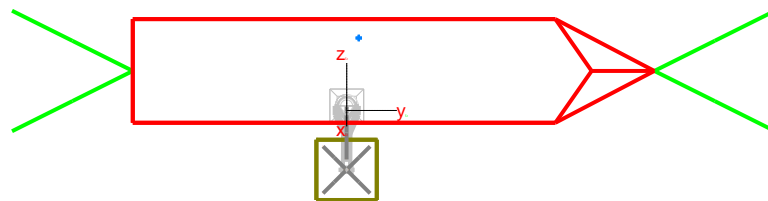


Figure C-2 Modal analysis: model of the coupled configuration – top view

Table C-1 Modal analysis coupling coefficients – Uncoupled system

Modal analysis 1 - Uncoupled	SURGE	SWAY	HEAVE	ROLL	PITCH	YAW	SURGE	SWAY	HEAVE	ROLL	PITCH	YAW	LUFFING
Period (s)	59.473	115.551	4.827	11.972	5.435	55.010	9.201	8.730	0.176	3.249	0.304	13.918	0.613
Frequency (Hz)	0.017	0.009	0.207	0.084	0.184	0.018	0.109	0.115	5.686	0.308	3.286	0.072	1.631
F3000; X (m)	0.993	0.000	-0.071	0.000	0.130	-0.014	-0.003	0.000	0.000	0.000	0.000	0.000	0.000
F3000; Y (m)	0.049	0.963	0.011	-0.027	-0.029	1.000	0.004	0.005	0.002	0.000	0.000	0.000	-0.003
F3000; Z (m)	0.001	0.000	0.997	0.001	-0.589	0.000	0.004	0.000	-0.004	0.000	0.000	0.000	0.290
F3000; RX (deg)	0.000	-0.005	0.012	-0.115	-0.066	-0.001	0.000	0.032	-0.002	0.000	0.000	0.000	0.072
F3000; RY (deg)	0.000	0.000	0.363	0.000	-0.661	0.000	0.002	0.000	-0.001	0.000	0.000	0.000	0.001
F3000; RZ (deg)	-0.026	0.013	-0.005	0.001	0.008	-0.518	-0.002	0.000	0.000	0.000	0.000	0.000	0.000
HookBuoy; X (m)	1.000	0.009	-0.243	0.003	0.624	-0.379	1.000	0.001	0.000	0.000	-0.001	0.000	0.000
HookBuoy; Y (m)	0.010	1.000	0.005	0.573	-0.055	0.207	-0.002	0.282	0.000	-0.003	0.000	0.000	0.020
HookBuoy; Z (m)	0.000	0.004	0.430	0.080	0.483	0.001	0.000	-0.022	1.000	0.000	0.000	0.000	-0.008
HookBuoy; RX (deg)	0.001	0.017	0.087	1.000	-0.697	0.016	-0.007	1.000	-0.001	1.000	0.000	0.000	0.200
HookBuoy; RY (deg)	0.000	0.000	0.390	0.000	-0.717	0.000	-0.033	0.000	-0.038	0.000	1.000	0.000	-0.001
HookBuoy; RZ (deg)	-0.027	0.013	0.001	0.002	-0.002	-0.553	0.002	0.002	0.000	0.001	0.000	1.000	0.004
BoomConstraint; RY (deg)	0.000	0.000	-0.004	-0.002	-0.006	0.000	0.000	0.000	0.094	0.000	0.000	0.000	-1.000

Table C-2 Modal analysis coupling coefficients – Constraint system, anti-heeling mass at the centre line

Modal analysis 2a - Constraint (pre-tension)	SURGE	SWAY	HEAVE	ROLL	PITCH	YAW	SURGE	SWAY	HEAVE	ROLL	PITCH	YAW	LUFFING
Period (s)	54.427	69.982	5.073	1.898	5.624	40.348	0.528	0.452	0.137	1.119	0.393	2.263	0.549
Frequency (Hz)	0.018	0.014	0.197	0.527	0.178	0.025	1.892	2.213	7.308	0.894	2.543	0.442	1.821
F3000; X (m)	0.393	-0.126	-0.052	-0.004	0.017	-0.388	0.000	0.000	0.000	0.000	0.000	0.000	0.000
F3000; Y (m)	0.920	0.159	0.054	-0.057	0.052	0.921	0.000	0.000	0.001	0.000	0.000	0.000	0.013
F3000; Z (m)	0.003	0.007	0.578	0.083	0.041	0.015	0.000	0.000	-0.002	0.000	0.000	0.000	0.000
F3000; RX (deg)	0.009	0.015	0.260	-0.296	0.282	0.008	0.000	0.000	-0.001	0.000	0.000	0.000	0.163
F3000; RY (deg)	0.000	0.001	0.270	0.019	-0.089	0.007	0.000	0.000	-0.001	0.000	0.000	0.000	0.001
F3000; RZ (deg)	-0.372	0.248	-0.002	0.000	0.001	-0.443	0.000	0.000	0.000	0.000	0.000	0.000	0.004
HookBuoy; X (m)	0.003	0.001	0.019	0.003	-0.006	-0.016	0.079	0.000	0.001	0.000	-0.002	0.000	0.022
HookBuoy; Y (m)	0.025	0.040	-0.037	0.042	-0.040	0.017	0.000	0.103	0.003	0.037	0.000	0.000	-0.001
HookBuoy; Z (m)	-0.001	-0.002	-0.007	0.074	-0.006	-0.001	0.000	0.000	1.000	0.000	0.000	0.000	0.122
HookBuoy; RX (deg)	-0.633	-0.999	0.912	-0.999	0.991	-0.429	0.000	1.000	-0.050	-1.000	0.000	0.002	0.676
HookBuoy; RY (deg)	0.052	0.021	0.410	0.042	-0.136	-0.269	1.000	0.000	0.020	0.000	1.000	0.004	0.267
HookBuoy; RZ (deg)	-0.058	0.037	-0.003	0.012	0.003	-0.061	0.002	-0.004	0.000	0.004	-0.009	1.000	-0.002
BoomConstraint; RY (deg)	0.000	0.001	-0.014	0.150	-0.014	0.000	0.001	0.002	0.060	-0.001	0.000	0.000	-1.000

Table C-3 Modal analysis coupling coefficients – Constraint system, anti-heeling mass at its final location

Modal analysis 2b - Constraint (pick-up)	SURGE	SWAY	HEAVE	ROLL	PITCH	YAW	SURGE	SWAY	HEAVE	ROLL	PITCH	YAW	LUFFING
Period (s)	39.852	61.363	5.022	1.844	5.663	27.274	0.481	0.591	0.136	0.430	0.334	1.084	0.543
Frequency (Hz)	0.025	0.016	0.199	0.542	0.177	0.037	2.080	1.691	7.354	2.324	2.997	0.923	1.843
F3000; X (m)	0.279	0.482	-0.054	-0.006	0.012	-0.415	0.000	0.000	0.000	0.000	0.000	0.000	0.000
F3000; Y (m)	0.904	0.876	0.036	-0.083	0.050	0.908	0.000	0.000	0.001	0.000	0.000	0.000	-0.001
F3000; Z (m)	0.022	-0.008	0.620	0.139	0.087	0.053	0.000	0.000	-0.002	0.000	0.000	0.000	0.001
F3000; RX (deg)	0.048	-0.013	0.242	-0.425	0.313	0.028	0.000	0.002	0.000	0.000	0.000	0.000	-0.015
F3000; RY (deg)	0.001	-0.001	0.306	0.031	-0.071	0.025	0.000	0.000	-0.001	0.000	0.000	0.000	0.000
F3000; RZ (deg)	-0.167	-0.675	0.004	0.000	0.002	-0.421	0.000	0.000	0.000	0.000	0.000	0.000	0.000
HookBuoy; X (m)	0.011	0.000	0.042	0.004	-0.010	-0.043	0.155	0.000	-0.001	0.000	0.013	0.000	0.000
HookBuoy; Y (m)	0.053	-0.014	-0.041	0.053	-0.053	0.019	0.000	0.050	0.000	0.042	0.000	0.000	0.049
HookBuoy; Z (m)	-0.006	0.001	-0.006	0.111	-0.006	-0.002	0.000	0.001	1.000	0.000	0.000	0.000	-0.013
HookBuoy; RX (deg)	-0.989	0.254	0.759	-0.997	0.989	-0.363	0.001	-1.000	-0.005	1.000	0.000	-0.001	-1.000
HookBuoy; RY (deg)	0.143	-0.003	0.651	0.072	-0.150	-0.578	1.000	0.000	-0.021	0.000	1.000	0.000	0.001
HookBuoy; RZ (deg)	-0.022	-0.085	0.001	-0.001	0.001	-0.054	0.000	-0.001	0.001	0.005	0.000	1.000	-0.001
BoomConstraint; RY (deg)	0.002	-0.001	-0.020	0.231	-0.022	0.001	0.000	-0.012	0.060	0.000	0.000	0.000	0.101

Table C-4 Modal analysis coupling coefficients – Coupled system

Modal Analysis 3 - Coupled	SURGE	SWAY	HEAVE	ROLL	PITCH	YAW	SURGE	SWAY	HEAVE	ROLL	PITCH	YAW	LUFFING
Period (s)	61.088	118.729	4.958	10.265	5.485	56.484	15.862	28.395	0.522	0.275	0.269	94.539	0.993
Frequency (Hz)	0.016	0.008	0.202	0.097	0.182	0.018	0.063	0.035	1.915	3.635	3.711	0.011	1.007
F3000; X (m)	0.912	0.000	-0.079	0.001	-0.095	0.012	-0.058	-0.001	0.000	0.000	0.000	0.000	0.000
F3000; Y (m)	-0.033	0.921	0.020	0.046	0.018	1.000	0.097	-0.194	-0.001	0.000	-0.002	0.006	0.000
F3000; Z (m)	0.002	0.000	0.997	-0.003	0.324	-0.001	0.021	0.001	0.000	0.000	0.000	-0.018	0.000
F3000; RX (deg)	0.001	-0.025	0.039	0.385	0.024	-0.019	0.010	-0.382	-0.014	0.000	0.000	0.003	0.043
F3000; RY (deg)	0.001	0.000	0.385	-0.001	0.467	0.000	0.012	0.000	0.000	0.000	0.000	-0.010	0.001
F3000; RZ (deg)	0.018	0.005	-0.007	0.007	-0.528	-0.049	0.031	0.000	0.000	0.000	0.000	-0.003	0.001
Topside; X (m)	1.000	0.004	-0.071	-0.002	-0.106	-0.401	1.000	0.033	0.000	0.000	-0.003	0.001	-0.004
Topside; Y (m)	-0.008	1.000	0.005	0.433	0.008	0.244	-0.001	0.960	0.000	-0.006	0.000	0.000	0.000
Topside; Z (m)	0.000	0.018	0.398	-0.280	-0.438	0.014	-0.004	0.279	0.013	0.000	0.000	-0.007	-0.029
Topside; RX (deg)	0.000	0.016	0.057	1.000	0.075	0.018	-0.001	0.276	0.006	0.250	0.000	-0.083	-0.852
Topside; RY (deg)	-0.061	0.000	0.860	0.005	0.997	0.029	-0.920	-0.009	0.000	0.000	-0.111	0.000	0.997
Topside; RZ (deg)	-0.013	0.015	0.000	0.000	0.294	0.001	-0.003	0.000	0.000	0.000	1.000	0.000	0.000
HookBuoy; X (m)	0.949	0.004	0.642	0.002	0.724	-0.378	0.233	0.025	0.000	0.000	0.028	0.001	0.777
HookBuoy; Y (m)	-0.007	0.986	-0.042	-0.415	-0.055	0.229	0.000	0.724	0.033	0.092	0.000	0.000	0.644
HookBuoy; Z (m)	0.000	0.018	0.392	-0.279	-0.433	0.014	-0.004	0.278	-0.004	0.000	0.000	0.000	-0.006
HookBuoy; RX (deg)	0.000	0.016	0.025	0.868	0.040	0.018	-0.001	0.272	-1.000	1.000	0.000	0.000	0.094
HookBuoy; RY (deg)	-0.028	0.000	0.377	0.001	0.499	0.013	-0.399	-0.004	-0.005	0.000	-1.000	0.000	-0.518
HookBuoy; RZ (deg)	-0.009	0.014	-0.001	0.001	-0.001	0.190	-0.005	0.001	0.002	0.004	0.000	0.874	-0.001
BoomConstraint; RY (deg)	0.000	-0.001	-0.020	0.002	0.020	-0.001	0.000	-0.010	0.098	0.000	0.000	0.000	-0.001

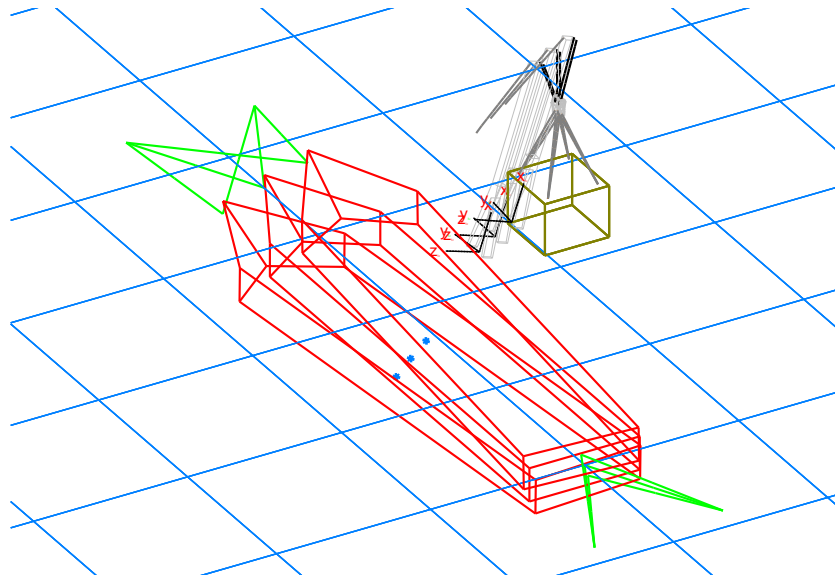


Figure C-3 Vessel surge mode – constraint model

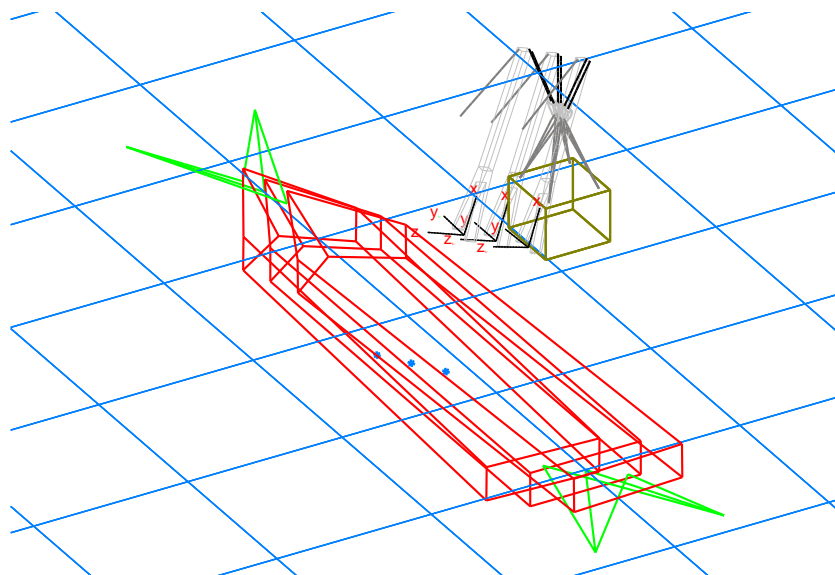


Figure C-4 Vessel sway mode – constraint model

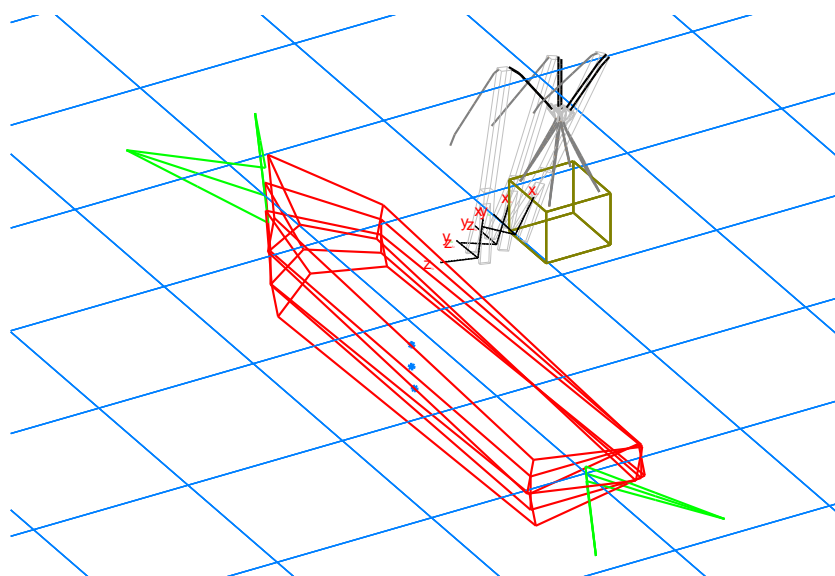


Figure C-5 Vessel heave mode – constraint model

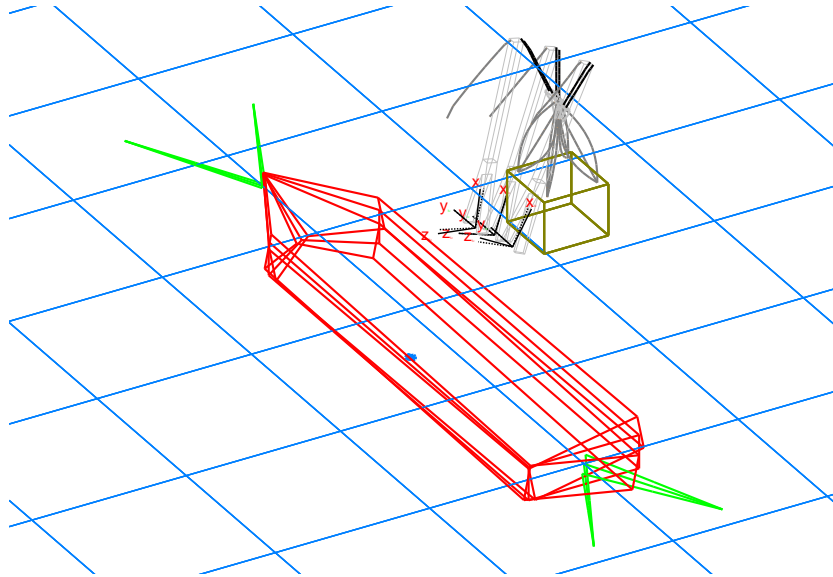


Figure C-6 Vessel roll mode – constraint model

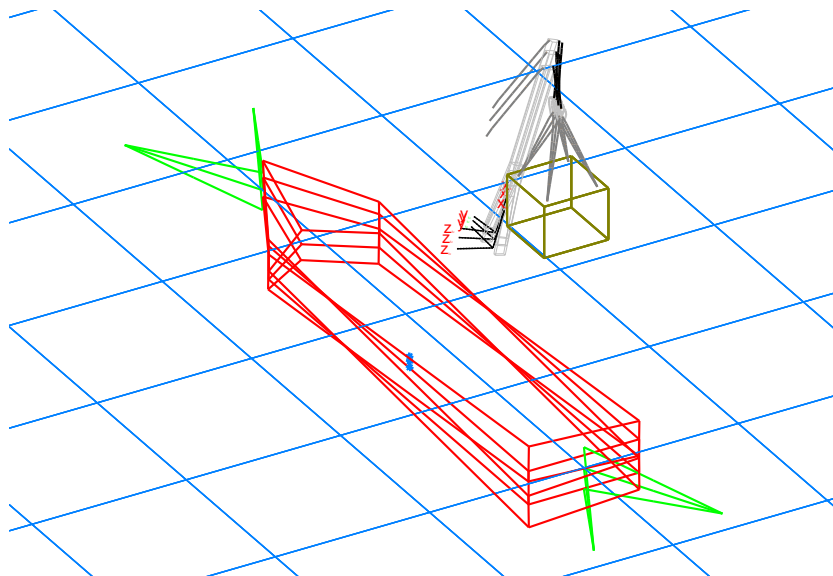


Figure C-7 Vessel pitch mode – constraint model

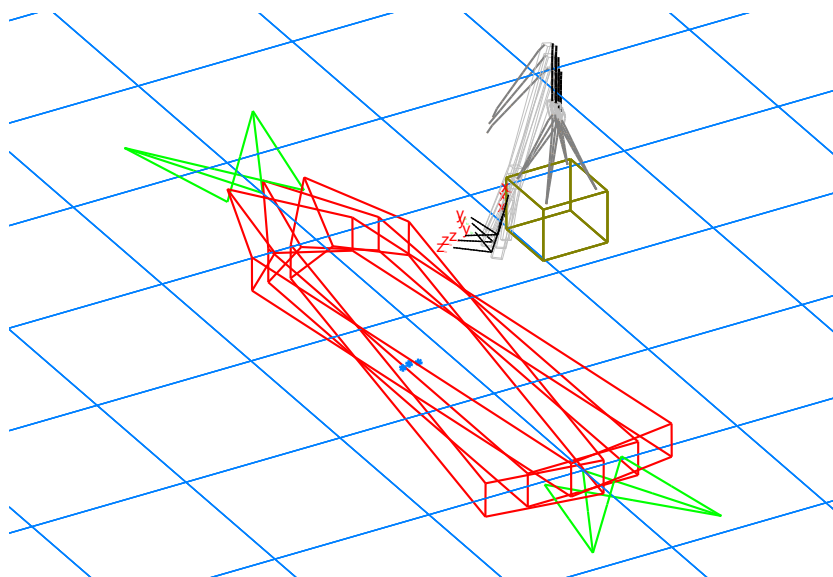


Figure C-8 Vessel yaw mode – constraint model

C.2. Pre-tensioning simulations

Table C-5 Mean of the maximum amplitudes snap loads [kN] per sea state

wave direction	180		210	
pre-tensioning scheme	regular	ASAP	regular	ASAP
Tp-2.2 Hs-0.5	694	511	595	445
Tp-3 Hs-1.0	1831	1499	1570	1574
Tp-4 Hs-1.5	1494	1369	1371	1191
Tp-5 Hs-2.5	1706	1612	1936	1702
Tp-6 Hs-3.0	2108	2353	2869	2686
Tp-7 Hs-3.0	3327	3202	2914	3222
Tp-8 Hs-3.0	4982	5324	4234	4076
Tp-9 Hs-2.0	4663	5167	3405	3855
Tp-10 Hs-1.5	2646	3498	3078	3229
Tp-11 Hs-1.0	2231	2802	2805	2608
Tp-12 Hs-1.0	1613	1514	2425	2534

Table C-6 Maximum amplitude snap loads [kN] per sea state

wave direction	180		210	
pre-tensioning scheme	regular	ASAP	regular	ASAP
Tp-2.2 Hs-0.5	929	810	784	624
Tp-3 Hs-1.0	2848	2585	2440	2515
Tp-4 Hs-1.5	1982	2167	2232	1959
Tp-5 Hs-2.5	2526	2177	2812	2383
Tp-6 Hs-3.0	4486	4862	4628	5452
Tp-7 Hs-3.0	6400	8126	6133	6694
Tp-8 Hs-3.0	11048	15403	10386	8498
Tp-9 Hs-2.0	10083	11181	7518	8070
Tp-10 Hs-1.5	8033	8489	5564	7121
Tp-11 Hs-1.0	6321	8011	6221	6141
Tp-12 Hs-1.0	3627	4084	5242	6569

C.3. Tension variation

Table C-7 Maximum amplitude of the tension variation

$\theta = 180$ [deg]	AH 20%	AH 40%	AH 60%	AH 80%	AH 100%
SHL [kN]	8873	13504	18152	22793	27429
Tp-2.2 Hs-0.5	428	881	865	953	1206
Tp-3 Hs-1.0	2725	1972	1412	1793	2407
Tp-4 Hs-1.5	2342	1683	1542	1641	1781
Tp-5 Hs-2.5	2447	2428	1698	1757	2009
Tp-6 Hs-3.0	2234	1697	1622	2044	1825
Tp-7 Hs-3.0	1784	1630	1232	1609	1523
Tp-8 Hs-3.0	2149	1406	1301	1385	1364
Tp-9 Hs-2.0	1359	1155	911	1069	1198
Tp-10 Hs-2.0	907	1093	847	1067	1107
Tp-11 Hs-1.5	498	1371	1137	1601	1604
Tp-12 Hs-1.0	700	1122	1370	1721	1957

Table C-8 Maximum amplitude of the tension variation

$\theta = 210$ [deg]	AH 20%	AH 40%	AH 60%	AH 80%	AH 100%
SHL [kN]	8873	13504	18151	22793	27429
Tp-2.2 Hs-0.5	369	857	929	932	928
Tp-3 Hs-1.0	2359	1735	1404	1783	1700
Tp-4 Hs-1.5	1759	1512	1396	1729	1590
Tp-5 Hs-2.5	2979	1931	1573	1730	1971
Tp-6 Hs-3.0	2351	1705	1597	2128	1535
Tp-7 Hs-3.0	1903	1457	1409	1571	1835
Tp-8 Hs-3.0	2305	1841	1411	1658	2253
Tp-9 Hs-2.0	1468	1049	1007	1270	1388
Tp-10 Hs-2.0	942	1052	893	1203	1457
Tp-11 Hs-1.5	683	901	900	1398	1669
Tp-12 Hs-1.5	1086	1467	1628	1807	2247

C.4. Lift simulations

Table C-9 Evaluation operational criteria – regular lift scheme - conical cut

$\theta = 180$ [deg]	DAF [-]	Offlead [kN]	Sidelead [kN]	Clearance TS-boom [m]	TS surge [m]	TS sway [m]	TS roll [deg]	TS pitch [deg]	TS yaw [deg]
criteria	1.233	1175	1175	3.00	1.50	1.50	2.00	2.00	3.00
Tp-2.2 Hs-0.5	1.015	101	60	4.25	0.18	0.26	0.14	0.07	0.40
Tp-3 Hs-1.0	1.016	113	234	4.25	0.18	0.26	0.15	0.37	0.77
Tp-4 Hs-1.5	1.016	104	196	4.25	0.18	0.26	0.15	0.30	0.69
Tp-5 Hs-2.5	1.021	146	208	4.24	0.23	0.29	0.27	0.35	0.79
Tp-6 Hs-3.0	1.047	396	299	4.07	0.50	0.53	0.48	0.77	2.98
Tp-7 Hs-2.0	1.043	324	469	4.02	0.94	0.59	0.57	1.56	2.29
Tp-7 Hs-3.0	1.081	584	718	3.77	1.01	1.02	1.24	1.45	7.28
Tp-8 Hs-2.0	1.078	449	836	3.96	1.23	0.54	0.65	2.64	3.78
Tp-8 Hs-3.0	1.136	979	1086	3.13	1.46	1.73	1.54	2.92	8.38
Tp-9 Hs-2.5	1.142	1062	1197	3.37	2.05	1.67	1.37	2.90	13.11
Tp-12 Hs-1.5	1.092	892	2062	2.69	3.98	2.09	1.75	4.88	15.00

Table C-10 Evaluation operational criteria – regular lift scheme - conical cut

$\theta = 210$ [deg]	DAF [-]	Offlead [kN]	Sidelead [kN]	Clearance TS-boom [m]	TS surge [m]	TS sway [m]	TS roll [deg]	TS pitch [deg]	TS yaw [deg]
criteria	1.233	1175	1175	3.00	1.50	1.50	2.00	2.00	3.00
Tp-2.2 Hs-0.5	1.016	108	59	4.24	0.18	0.26	0.15	0.06	0.39
Tp-3 Hs-1.0	1.016	138	203	4.24	0.18	0.26	0.18	0.31	0.73
Tp-4 Hs-1.5	1.016	168	138	4.24	0.19	0.26	0.21	0.22	0.61
Tp-5 Hs-2.5	1.022	167	180	4.23	0.23	0.28	0.37	0.34	1.16
Tp-6 Hs-3.0	1.058	379	318	3.71	0.44	0.86	0.90	0.90	2.35
Tp-7 Hs-2.0	1.052	287	377	3.91	0.58	0.48	0.65	1.05	1.62
Tp-7 Hs-3.0	1.081	899	814	3.46	1.14	1.51	1.32	2.45	7.14
Tp-8 Hs-2.0	1.056	586	760	3.68	1.05	0.85	1.30	1.88	5.58
Tp-8 Hs-3.0	1.206	991	1336	2.88	1.84	1.54	1.94	3.41	11.32
Tp-9 Hs-2.0	1.142	1031	1355	2.95	1.91	1.97	2.01	3.14	12.90
Tp-12 Hs-1.0	1.088	1232	1181	2.28	2.36	2.16	2.74	2.97	19.09

Table C-11 Maximum crane loads – ASAP lift scheme - conical cut

$\theta = 180$ [deg]	DAF [-]	Offlead [kN]	Sidelead [kN]	Clearance TS-boom [m]	TS surge [m]	TS sway [m]	TS roll [deg]	TS pitch [deg]	TS yaw [deg]
criteria	1.233	1175	1175	3.00	1.50	1.50	2.00	2.00	3.00
Tp-7 Hs-2.0	1.038	401	447	4.01	0.71	0.84	0.52	1.13	2.95
Tp-7 Hs-3.0	1.064	513	669	3.70	1.31	1.08	1.09	2.04	5.70

Table C-12 Maximum crane loads – ASAP lift scheme - conical cut

$\theta = 210$ [deg]	DAF [-]	Offlead [kN]	Sidelead [kN]	Clearance TS-boom [m]	TS surge [m]	TS sway [m]	TS roll [deg]	TS pitch [deg]	TS yaw [deg]
criteria	1.233	1175	1175	3.00	1.50	1.50	2.00	2.00	3.00
Tp-7 Hs-2.0	1.044	498	38	3.70	0.61	1.01	0.77	1.21	2.95
Tp-7 Hs-3.0	1.065	620	848	3.51	1.44	1.37	1.44	2.30	6.04

Table C-13 Maximum crane loads – regular lift scheme - carousel cut

$\theta = 180$ [deg]	DAF [-]	Offlead [kN]	Sidelead [kN]	Clearance TS-boom [m]	TS surge [m]	TS sway [m]	TS roll [deg]	TS pitch [deg]	TS yaw [deg]
criteria	1.233	1175	1175	3.00	1.50	1.50	2.00	2.00	3.00
Tp-7 Hs-2.0	1.063	297	406	4.11	0.55	0.37	0.44	0.93	1.52
Tp-7 Hs-3.0	1.086	496	965	3.55	1.28	1.19	0.84	2.38	6.68

Table C-14 Maximum crane loads – regular lift scheme - carousel cut

$\theta = 210$ [deg]	DAF [-]	Offlead [kN]	Sidelead [kN]	Clearance TS-boom [m]	TS surge [m]	TS sway [m]	TS roll [deg]	TS pitch [deg]	TS yaw [deg]
criteria	1.233	1175	1175	3.00	1.50	1.50	2.00	2.00	3.00
Tp-7 Hs-2.0	1.052	287	377	3.91	0.58	0.48	0.65	1.05	1.62
Tp-7 Hs-3.0	1.087	537	720	3.77	0.90	0.87	1.02	2.25	4.44